Available online at www.sciencedirect.com
SCIENCE DIRECT®
Journal of Computational Physics 207 (2005) 660–694
JOURNAL OF COMPUTATIONAL PHYSICS
www.elsevier.com/locate/jcp

Multilevel schemes for the shallow water equations

T. Dubois [a], F. Jauberteau [b,*], R.M. Temam [c,d], J. Tribbia [e]

[a] *Laboratoire de Mathématiques Appliquées, Université Clermont-Ferrand 2, CNRS UMR 6620, 63177 Aubière, France*
[b] *Laboratoire de Mathématiques, Université de Nantes, CNRS UMR 6629, BP 92208, 44322 Nantes, France*
[c] *Laboratoire de Mathématiques, Université Paris Sud, CNRS UMR 8628, Bâtiment 425, 91405 Orsay, France*
[d] *The Institute for Applied Mathematics and Scientific Computing, Indiana University, Rawles Hall, Bloomington, IN 47405, USA*
[e] *National Center for Atmospheric Research (NCAR), Climate and Global Dynamics Division, Boulder, CO 80305, USA*

Received 27 October 2003; received in revised form 28 March 2004; accepted 29 January 2005
Available online 17 March 2005

Abstract

In this paper, we study a number of multilevel schemes for the numerical solution of the shallow water equations; new schemes and new perspectives of known schemes are examined. We consider the case of periodic boundary conditions. Spatial discretization is obtained using a Fourier spectral Galerkin method. For the time integration, two strategies are studied. The first one is based on scale separation, and we choose the time scheme (explicit or semi-implicit) as a function of the spatial scales (multilevel schemes). The second approach is based on a splitting of the operators, and we choose the time integration method as a function of the operator considered (multistep or fractional schemes). The numerical results obtained are compared with the explicit reference scheme (Leap–Frog scheme), and with the semi-implicit scheme (Leap–Frog scheme with Crank–Nicholson scheme for the gravity terms), both computed with a similar mesh. The drawback of the explicit reference scheme being the numerical stability constraint on the time step, and the drawback of the semi-implicit scheme being the dispersive error, the aim with the new schemes is to obtain schemes with less dispersive error than the semi-implicit scheme, and with better stability properties than the explicit reference scheme. The numerical results obtained show that the schemes proposed allow one to reduce the dispersive error and to increase the numerical stability at reduced cost.

Keywords: Multilevel methods; Shallow water equations; Fractional step methods; Inertial waves; Gravity waves

* Corresponding author. Tel.: +33 2 51 12 59 31; fax: +33 2 51 12 59 12.
E-mail addresses: Thierry.Dubois@math.univ-bpclermont.fr (T. Dubois), Francois.Jauberteau@math.univ-nantes.fr (F. Jauberteau), Roger.Temam@math.u-psud.fr (R.M. Temam), tribbia@ucar.edu (J. Tribbia).

0021-9991/$ - see front matter © 2005 Elsevier Inc. All rights reserved.
doi:10.1016/j.jcp.2005.01.025

1. Introduction: motivation of the problem

We consider the two-dimensional nonlinear shallow water problem, with periodic boundary conditions (doubly periodic f-plane). This problem is considered as a planetary model for the simulation of atmospheric or oceanic flows. The equations are written as follows:

$$\begin{aligned} &\frac{\partial \mathbf{u}}{\partial t} + (\mathbf{\Omega} \times \mathbf{u}) + f\mathbf{u}^{\perp} + \nabla\left(gh + \frac{1}{2}|\mathbf{u}|^2\right) = 0, \\ &\frac{\partial h}{\partial t} + \operatorname{div}((H+h)\mathbf{u}) = 0, \end{aligned} \tag{1.1}$$

where $\mathbf{u} = (u, v)^{\top}$ is the velocity field, $\mathbf{u}^{\perp} = (-v, u)^{\top}$ the orthogonal velocity field, $\mathbf{\Omega} = \nabla \times \mathbf{u}$ the vorticity vector, h the height of the free surface around H, and $|-|$ the Euclidean norm.

Here, we have considered the formulation of the shallow water problem with the following scalar dependent variables instead of the velocity vector $\mathbf{u}$: the *vorticity* $\omega = \frac{\partial v}{\partial x} - \frac{\partial u}{\partial y}$ and the *plane divergence* $\delta = \frac{\partial u}{\partial x} + \frac{\partial v}{\partial y}$. So, the problem considered is as follows:

$$\begin{aligned} &\frac{\partial \omega}{\partial t} + \frac{\partial(\omega u)}{\partial x} + \frac{\partial(\omega v)}{\partial y} + f\delta = 0, \\ &\frac{\partial \delta}{\partial t} + \frac{\partial(\omega u)}{\partial y} - \frac{\partial(\omega v)}{\partial x} - f\omega + \Delta\left(gh + \frac{1}{2}|\mathbf{u}|^2\right) = 0, \\ &\frac{\partial h}{\partial t} + H\delta + \operatorname{div}(h\mathbf{u}) = 0. \end{aligned} \tag{1.2}$$

It is necessary to supplement these equations with initial conditions for ω, δ, h, and boundary conditions (periodicity in the two directions). The computational domain Ω considered is $\Omega = (0, L_x) \times (0, L_y)$, with $L_x = L_y = 6.31 \times 10^6$ m (earth radius), the period in the x and y directions.

The problem (1.2) induces substantial numerical difficulties if we want to compute directly the numerical approximation of (1.2). Indeed, most atmospheric flows are turbulent flows, i.e., they contain a wide range of scales with very different spatial size and characteristic times. To overcome these numerical difficulties, large eddy simulation (LES) models for turbulence modeling are usually proposed, in order to compute only the large scales of the flow (which contain most of the kinetic energy and the enstrophy in two-dimensional turbulent flows), and modeling the dissipative action of the small scales (which are not computed) on the large ones (see, for example [36,39] for more details). In meteorology, a model often used consists in adding a hyperdissipative operator in Eqs. (1.2) (see [3,5,6,21,35,44]). Such an operator is of the form:

$$\nu_{\mathrm{T}} \Delta^{2p} \tag{1.3}$$

with p an integer parameter and ν_{T} the turbulent viscosity (or eddy viscosity):

$$\nu_{\mathrm{T}} = \frac{\zeta}{k'^{4p}_{\max} \Delta t}. \tag{1.4}$$

Here, Δt is the time step retained for the numerical computation, $k'_{\max}$ is the modulus of the highest wavenumber associated with the smallest computed scales: $k'_{\max} = \sqrt{2}\frac{2\pi}{L_x}\left(\frac{N}{2}\right) = \sqrt{2}\frac{2\pi}{L_y}\left(\frac{N}{2}\right)$, ζ is a nondimensional positive constant and p is an integer as in (1.3). In practice, for the numerical simulations described in this paper, we have chosen $p = 2$ and $\zeta = 10^4$.

As we will see in the next section, the role of the additive term (1.3) in Eqs. (1.2) is to prevent spectral reflections in the high wavenumbers of the spectra, in order to obtain an energy spectrum (velocity spectrum) with a slope of k'^{-3} in the inertial range, in agreement with the two-dimensional homogeneous

turbulence theory (see [27]). The slope of the spectrum associated with the height is k'^{-5}, since h appears through a gradient in the velocity equation (1.1) (see [14]). Finally, the problem considered here can be written as follows:

$$\begin{aligned}
&\frac{\partial\omega}{\partial t}+\nu_{\mathrm{T}}\Delta^{2p}\omega+\frac{\partial(\omega u)}{\partial x}+\frac{\partial(\omega v)}{\partial y}+f\delta=0,\\
&\frac{\partial\delta}{\partial t}+\nu_{\mathrm{T}}\Delta^{2p}\delta+\frac{\partial(\omega u)}{\partial y}-\frac{\partial(\omega v)}{\partial x}-f\omega+\Delta\left(gh+\frac{1}{2}|\mathbf{u}|^2\right)=0,\\
&\frac{\partial h}{\partial t}+\nu_{\mathrm{T}}\Delta^{2p}h+H\delta+\operatorname{div}(h\mathbf{u})=0.
\end{aligned}\tag{1.5}$$

For the spatial discretization, we have used a spectral Galerkin method (see [8,22]), with the trigonometric polynomials as Galerkin basis since the boundary conditions are periodic (Fourier spectral Galerkin method). Since ω, δ and h are periodic in space, we can consider the infinite Fourier expansion for these dependent variables. If the dependent variables are regular, the Fourier coefficients $\hat{\omega}_{\mathbf{k}}$, $\hat{\delta}_{\mathbf{k}}$ and $\hat{h}_{\mathbf{k}}$ decrease rapidly when $|\mathbf{k}|$ increases (see [8,22] for example). So, we can look for an approximation of ω, δ and h of the following form (truncated Fourier expansions):

$$\begin{aligned}
&\omega_N(\mathbf{x},t)=\sum_{\mathbf{k}\in\mathbb{I}_N}\hat{\omega}_{\mathbf{k}}(t)\exp(\mathrm{i}\mathbf{k}'\cdot\mathbf{x}),\\
&\delta_N(\mathbf{x},t)=\sum_{\mathbf{k}\in\mathbb{I}_N}\hat{\delta}_{\mathbf{k}}(t)\exp(\mathrm{i}\mathbf{k}'\cdot\mathbf{x}),\\
&h_N(\mathbf{x},t)=\sum_{\mathbf{k}\in\mathbb{I}_N}\hat{h}_{\mathbf{k}}(t)\exp(\mathrm{i}\mathbf{k}'\cdot\mathbf{x}),
\end{aligned}\tag{1.6}$$

where $\mathbf{k}=(k_1,k_2)$, $\mathbf{k}'=(k_1',k_2')=(\frac{2\pi}{L_x}k_1,\frac{2\pi}{L_y}k_2)$, $\mathbf{x}=(x,y)$, $\mathbf{k}'\cdot\mathbf{x}=k_1'x+k_2'y$ is the Euclidean scalar product and with $\mathbb{I}_N=[1-N/2,N/2]^2$. The total number of modes retained is N^2. We have retained the same number of modes N in the two directions x and y, since the computational domain Ω is symmetric ($L_x=L_y$), and the turbulence is homogeneous and isotropic (see [4]). Moreover, we note that for ω_N, δ_N and h_N defined in (1.6), the periodic boundary conditions are automatically satisfied (Galerkin approximation).

The Fourier coefficients are computed using a method of weighted residuals (MWR). We impose that the residuals, obtained by substituting ω_N, δ_N and h_N, to ω, δ and h, in (1.5), have an orthogonal projection on the space $V_N=\operatorname{Span}\{\exp(\mathrm{i}\mathbf{k}'\cdot\mathbf{x}),\ \mathbf{k}\in\mathbb{I}_N\}$ equal to zero, for the scalar product $(-,-)_{L^2(\Omega)}$ defined in $L^2(\Omega)$. This is equivalent to minimizing the residuals in energy norm (least square method), i.e., for the norm $\|-\|_{L^2(\Omega)}$ associated with the previous scalar product. So, using the orthogonality properties of the Fourier polynomials for the $L^2(\Omega)$ scalar product, we obtain the following system of ordinary differential equations (ODEs), for the Fourier coefficients $\hat{\omega}_{\mathbf{k}}$, $\hat{\delta}_{\mathbf{k}}$ and $\hat{h}_{\mathbf{k}}$, $\mathbf{fk}\in\mathbb{I}_N$:

$$\begin{aligned}
&\frac{\mathrm{d}}{\mathrm{d}t}\hat{\omega}_{\mathbf{k}}+\nu_{\mathrm{T}}|\mathbf{k}'|^{4p}\hat{\omega}_{\mathbf{k}}+\hat{T}_{\omega,N}(\mathbf{k})+f\hat{\delta}_{\mathbf{k}}=0,\\
&\frac{\mathrm{d}}{\mathrm{d}t}\hat{\delta}_{\mathbf{k}}+\nu_{\mathrm{T}}|\mathbf{k}'|^{4p}\hat{\delta}_{\mathbf{k}}+\hat{T}_{\delta,N}(\mathbf{k})-f\hat{\omega}_{\mathbf{k}}-g|\mathbf{k}'|^2\hat{h}_{\mathbf{k}}=0,\\
&\frac{\mathrm{d}}{\mathrm{d}t}\hat{h}_{\mathbf{k}}+\nu_{\mathrm{T}}|\mathbf{k}'|^{4p}\hat{h}_{\mathbf{k}}+H\hat{\delta}_{\mathbf{k}}+\hat{T}_{h,N}(\mathbf{k})=0.
\end{aligned}\tag{1.7}$$

With spectral Galerkin methods, one of the difficulties is the computation of the nonlinear terms. We have denoted by $T_{\omega,N}$, $T_{\delta,N}$ and $T_{h,N}$ the approximations of these nonlinear convective terms:

$$
\begin{aligned}
T_{\omega,N} &= \frac{\partial}{\partial x}(\omega_N u_N) + \frac{\partial}{\partial y}(\omega_N v_N),\\
T_{\delta,N} &= \frac{\partial}{\partial y}(\omega_N u_N) - \frac{\partial}{\partial x}(\omega_N v_N) + \frac{1}{2}\Delta(|\mathbf{u_N}|^2),\\
T_{h,N} &= \operatorname{div}(h_N \mathbf{u_N}).
\end{aligned}
\tag{1.8}
$$

For the computation of the Fourier coefficients $\hat{T}_{\omega,N}(\mathbf{k})$, $\hat{T}_{\delta,N}(\mathbf{k})$ and $\hat{T}_{h,N}(\mathbf{k})$ of the nonlinear terms, we use a pseudospectral method (see [8,22]). In this way, the total number of operations required to compute the nonlinear terms is $O(N^2 \log_2(N))$ operations. The evaluation of the Fourier coefficients of the three nonlinear terms (1.8) of the shallow water problem (1.5) requires 9 FFTs (direct and inverse), at each time step. To eliminate the aliasing error we use the 3/2 rule (see [8]).

For the time integration of the previous system of ODEs (1.7), we shall consider two time schemes: an explicit scheme and a semi-implicit scheme. The trigonometric polynomials being eigenfunctions of the hyperdissipative operator (1.3) used for the turbulence modeling, the matrix obtained is diagonal. So an exact time integration of the dissipative terms can be obtained, with no restrictive stability constraint (see [8,15]). We will now describe the two proposed schemes, which are, respectively, explicit and semi-implicit for the lower order and nonlinear terms; both solve exactly the hyperdissipative part.

1.1. Explicit scheme

Classically, in meteorology, the Leap–Frog scheme, which is a second order explicit scheme, is used for the time integration of the rotation, convective and gravity terms (see [18,49] for example). In the present case, we obtain, $\forall \mathbf{k} \in \mathbb{I}_N$:

$$
\begin{aligned}
\hat{\omega}_{\mathbf{k}}^{n+1} &= \exp(-2\nu_T \Delta t |\mathbf{k}'|^{4p}) \hat{\omega}_{\mathbf{k}}^{n-1} - 2\Delta t \exp(-\nu_T \Delta t |\mathbf{k}'|^{4p})(\hat{T}_{\omega,N}^{n}(\mathbf{k}) + f\hat{\delta}_{\mathbf{k}}^{n}),\\
\hat{\delta}_{\mathbf{k}}^{n+1} &= \exp(-2\nu_T \Delta t |\mathbf{k}'|^{4p}) \hat{\delta}_{\mathbf{k}}^{n-1} - 2\Delta t \exp(-\nu_T \Delta t |\mathbf{k}'|^{4p})(\hat{T}_{\delta,N}^{n}(\mathbf{k}) - f\hat{\omega}_{\mathbf{k}}^{n} - |\mathbf{k}'|^2 g\hat{h}_{\mathbf{k}}^{n}),\\
\hat{h}_{\mathbf{k}}^{n+1} &= \exp(-2\nu_T \Delta t |\mathbf{k}'|^{4p}) \hat{h}_{\mathbf{k}}^{n-1} - 2\Delta t \exp(-\nu_T \Delta t |\mathbf{k}'|^{4p})(\hat{T}_{h,N}^{n}(\mathbf{k}) + H\hat{\delta}_{\mathbf{k}}^{n}),
\end{aligned}
\tag{1.9}
$$

where Δt is the time step retained for the time integration. Using the classical von Neumann stability analysis (see [37,49]), we obtain the stability constraint for this explicit scheme:

$$
\left| |\mathbf{U}| \pm \sqrt{gH + f^2 \frac{1}{k'^2}} \right| \Delta t k' \leqslant 1,
\tag{1.10}
$$

where $k' = |\mathbf{k}'|$, $\mathbf{U} = (U, V)$ is a constant advecting velocity (linearized problem), with $|-|$ the Euclidean norm, and the mesh size $\Delta x = L_x/N = L_y/N$. In practice, for the numerical simulation described in Section 3.1, we have retained $N = 256$ and $\Delta t = 10$ s.

From (1.10) we can derive three stability conditions, depending on which term is dominant in the left-hand side of (1.10). The first stability constraint, denoted by $Stab_1$, is due to the explicit treatment of the convective terms (i.e., when $|\mathbf{U}|$ is large compared to $\sqrt{gH}$ and fL, high Rossby number, high speed flow). This is the CFL condition:

$$
Stab_1 : \quad |\mathbf{U}| \Delta t k' \leqslant 1.
\tag{1.11}
$$

The second stability constraint, denoted by $Stab_2$, comes from the explicit treatment of the inertial terms associated with the rotation of the earth (Coriolis force, i.e., when fL is large compared to $|\mathbf{U}|$ and $\sqrt{gH}$, high rotation or very small Rossby number):

$$
Stab_2 : \quad f \Delta t \leqslant 1.
\tag{1.12}
$$

Finally, the third stability condition, called $Stab_3$, is due to the explicit treatment of the gravity terms $g\Delta h$ and $H\delta$ in (1.9), (i.e., when $\sqrt{gH}$ is large compared to fL and $|\mathbf{U}|$, that is gravity dominated flows):

$$Stab_3: \quad \sqrt{gH}\Delta t k' \leqslant 1. \tag{1.13}$$

Generally, we have $|\mathbf{U}| \simeq 10$–100 m/s (Jet-Stream), $g = 9.81$ m/s^2, $H = 10^4$ m (troposphere) and the Coriolis force $f = 10^{-4}$ s^{-1}. So the more restrictive stability constraint in (1.10) is the condition $Stab_3$ defined in (1.13). Moreover, we see that the stability constraint $Stab_3$ is more restrictive for the high wavenumbers k' than for the small wavenumbers. So, the explicit scheme (1.9) is more stable for the computation of the large scales (small wavenumbers).

1.2. Semi-implicit scheme

To increase the stability of the explicit scheme (1.9) a second order implicit scheme (Crank–Nicholson scheme) is used for the time integration of the gravity terms $g\Delta h$ and $H\delta$, and a second order explicit scheme (Leap–Frog scheme) is used for the rotation and convective terms (see [18,38,49]). In the present case, we obtain the following second order semi-implicit scheme, $\forall \mathbf{k} \in \mathbb{I}_N$:

$$\begin{aligned}
&\hat{\omega}_{\mathbf{k}}^{n+1} = \exp(-2\nu_{\mathrm{T}}\Delta t|\mathbf{k}'|^{4p})\hat{\omega}_{\mathbf{k}}^{n-1} - 2\Delta t\exp(-\nu_{\mathrm{T}}\Delta t|\mathbf{k}'|^{4p})(\hat{T}_{\omega,N}^{n}(\mathbf{k}) + f\hat{\delta}_{\mathbf{k}}^{n}),\\
&\hat{\delta}_{\mathbf{k}}^{n+1} - g\Delta t|\mathbf{k}'|^2\hat{h}_{\mathbf{k}}^{n+1} = g\Delta t|\mathbf{k}'|^2\exp(-2\nu_{\mathrm{T}}\Delta t|\mathbf{k}'|^{4p})\hat{h}_{\mathbf{k}}^{n-1} + \exp(-2\nu_{\mathrm{T}}\Delta t|\mathbf{k}'|^{4p})\hat{\delta}_{\mathbf{k}}^{n-1}\\
&\qquad\qquad - 2\Delta t\exp(-\nu_{\mathrm{T}}\Delta t|\mathbf{k}'|^{4p})(\hat{T}_{\delta,N}^{n}(\mathbf{k}) - f\hat{\omega}_{\mathbf{k}}^{n}),\\
&\hat{h}_{\mathbf{k}}^{n+1} + H\Delta t\hat{\delta}_{\mathbf{k}}^{n+1} = -H\Delta t\exp(-2\nu_{\mathrm{T}}\Delta t|\mathbf{k}'|^{4p})\hat{\delta}_{\mathbf{k}}^{n-1} + \exp(-2\nu_{\mathrm{T}}\Delta t|\mathbf{k}'|^{4p})\hat{h}_{\mathbf{k}}^{n-1}\\
&\qquad\qquad - 2\Delta t\exp(-\nu_{\mathrm{T}}\Delta t|\mathbf{k}'|^{4p})\hat{T}_{h,N}^{n}(\mathbf{k}).
\end{aligned} \tag{1.14}$$

The stability constraint for the semi-implicit scheme (1.14), obtained with the von Neumann stability analysis, is:

$$\left||\mathbf{U}| \pm \sqrt{gH(\cos(\mu\Delta t))^2 + f^2\frac{1}{k'^2}}\right|\Delta t k' = \sin(\mu\Delta t) \leqslant 1, \tag{1.15}$$

with $\mu = -\mathbf{k}'\cdot\mathbf{U}$ or $\mu = -\mathbf{k}\prime\cdot\mathbf{U} \pm \sqrt{gHk'^2 + f^2}$ (frequencies associated with wave propagation, see [37,49]). In practice, for the numerical simulation described in Section 3.2, we have retained $N = 256$ and $\Delta t = 50$ s.

By comparison with (1.10), the term $(\cos(\mu\Delta t))^2$ reduces the stability constraint due to the gravity terms. In practice, for a similar spatial resolution, we can choose, at least, a time step five times larger for the semi-implicit scheme (1.14) than for the explicit scheme (1.9). However, the drawback of the semi-implicit scheme is that the increase of the stability is obtained by reducing the speed of the wave propagation (dispersive error). Moreover, this slow down, produced by the semi-implicit scheme, is more important on the high wavenumbers than on the low wavenumbers (see [49] and Fig. 2(a)).

The aim of this paper is to propose new numerical schemes, accurate and with good stability properties, in order to increase the time step needed by comparison with the explicit scheme (1.9), and so to decrease the CPU time required for the numerical simulations, and with less dispersive error than for the semi-implicit scheme (1.14). The stability constraint (1.13) is function of the wavenumber, and the explicit scheme (1.9) is more stable for the small wavenumbers than for the large wavenumbers. So we are lead to consider a scale separation, and to adapt the time integration to the wavenumbers computed (i.e., to the size of the scales computed). Such schemes are called *multilevel schemes*. Multilevel methods have been previously developed for the Navier–Stokes equations, in the case of homogeneous isotropic turbulence and in the case of the channel flow problem (see, for example [15–17]).

Another possibility is as follows: since the stability constraint is function of the parts of the shallow water problem (1.5), i.e., $Stab_1$ for the convective terms (see (1.11)), $Stab_2$ for the rotations terms (see (1.12)), and $Stab_3$ for the gravity terms (see (1.13)), we can separate the terms (splitting of the operators), in order to adapt the time integration scheme to the terms integrated (i.e., to the operator integrated). Such schemes are called *multistep methods* or *fractional step methods*. For previous works see, for example [2,7,19,25,26,28–30,40,41]. By difference with the time split schemes proposed in Section 4, in which we use only one time step, the time split schemes described in the previous references are a form of partial operator splitting employing two different time steps. The split schemes identify the terms responsible for the rapid oscillations and integrate them in time, with small time step, while holding the other terms constant. The result of this integration is then used to advance the other terms with a larger time step, well appropriate to describe the slower motion. A variant is proposed in [31], which integrates the fast problem using a low order scheme with small time step, and then average the result on a long time step to use in a high order accurate integration of the slow variables.

This paper is organized as follows. In Section 2, we describe some schemes based on a splitting of the scales (multilevel methods), and the numerical results obtained with such schemes are presented in Section 3. Then, in Section 4, we propose some schemes based on a splitting of the operators (multistep or fractional step methods), and the numerical results obtained with such schemes are described in Section 5. Finally, Section 6 contains some concluding remarks and indications on future developments.

2. New schemes based on a splitting of the scales (multilevel methods)

In this section, we shall describe new schemes based on a splitting of the scales, and an adaptation of the time scheme used (explicit scheme (1.9) or semi-implicit scheme (1.14)) according to the size of the scales computed. Following Section 1, the aim is to obtain new schemes, more accurate than the semi-implicit scheme (1.14) (less dispersive error), and with better stability properties than the explicit scheme (1.9).

The shallow water problem can be viewed as a surrogate for global primitive equation models which do not generally filter the Lamb wave that can be viewed either as a horizontally propagating acoustic wave or an inertia gravity wave. The high wavenumber behavior of the Lamb wave is well approximated with the shallow water system. Note that the Lamb wave may not be relevant for high resolution limited area models which filter this mode and bound the highest frequency of atmospheric waves by the Brunt–Vaisala frequency.

In the shallow water problem (1.1), there are present the propagation at a constant speed $\mathbf{U}$ due to the convective terms (linearized problem), the propagation of the inertial waves due to the inertial or rotation terms (Coriolis force), and the propagation of the gravity waves due to the gravity terms. The frequencies (phase speed), associated with these propagation speeds, can be written as (see [24,49]):

$$\begin{aligned}
\mu_{1,\mathbf{k}} &= -\mathbf{U}\cdot\mathbf{k}', \\
\mu_{2,\mathbf{k}} &= -\left(\mathbf{U}\cdot\mathbf{k}' + \sqrt{gHk'^2 + f^2}\right), \\
\mu_{3,\mathbf{k}} &= -\left(\mathbf{U}\cdot\mathbf{k}' - \sqrt{gHk'^2 + f^2}\right).
\end{aligned} \tag{2.1}$$

When $k = |\mathbf{k}|$ increases, $|\mu_{1,\mathbf{k}}|$, $|\mu_{2,\mathbf{k}}|$ and $|\mu_{3,\mathbf{k}}|$ increase. Moreover, $|\mu_{1,\mathbf{k}}| \ll |\mu_{i,\mathbf{k}}|$ for $i = 2, 3$, and $|\mu_{2,\mathbf{k}}| \simeq |\mu_{3,\mathbf{k}}|$ (see Fig. 1). As it has been previously said, the dispersive error (slow down) is more important on the high wavenumbers than on the low wavenumbers. To illustrate this, let us consider the following equation:

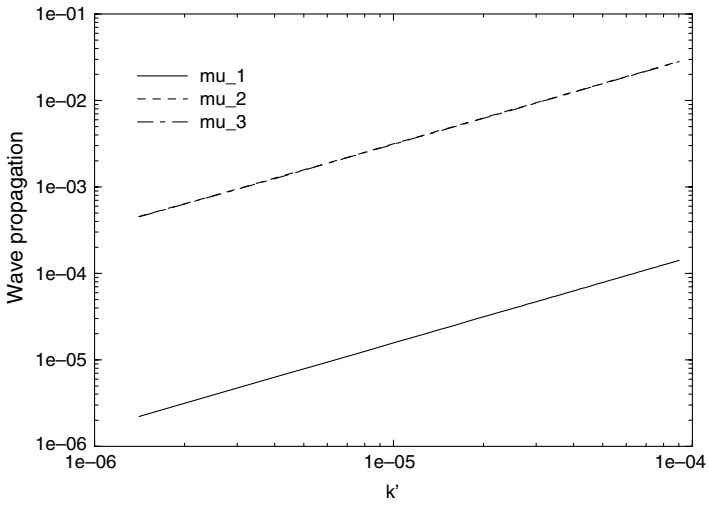

Fig. 1. Frequencies (phase speed) $\mu_{1,\mathbf{k}}$, $\mu_{2,\mathbf{k}}$ and $\mu_{3,\mathbf{k}}$ according (2.1).

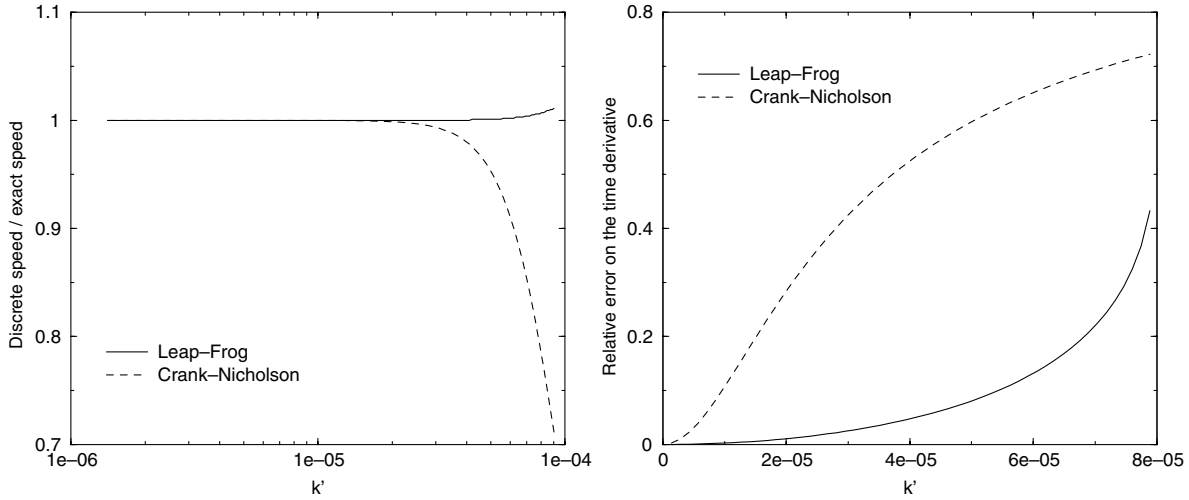

Fig. 2. Error on the wave propagation speed (dispersive error), and relative error on the time derivative, due to time integration scheme. We have used a time step five times larger for the Crank–Nicholson scheme than for the Leap–Frog scheme.

$$\frac{\partial q_k}{\partial t} + c\frac{\partial q_k}{\partial x} = 0, \tag{2.2}$$

associated with the propagation of a wave at a speed $c = \sqrt{gH}$:

$$q_k(x,t) = Q_k \exp(\mathrm{i}k'(x - ct)), \tag{2.3}$$

with $k' = \frac{2\pi}{L_x}k$. If we discretize (2.2) using the Leap–Frog scheme, we shall obtain a propagation speed for the computed solution equal to:

$$c_{\mathrm{LF},k} = \frac{1}{k'\Delta t}\arcsin(c\Delta t k'), \tag{2.4}$$

where Δt is a time step insuring the stability of the Leap–Frog scheme: $c\Delta t\, k' \leqslant 1$ (see (1.10)).

Now, if we consider the discretization of (2.2), using the Crank–Nicholson scheme, we shall obtain a propagation speed for the computed solution equal to:

$$c_{\mathrm{CN},k} = \frac{1}{k'\Delta t}\operatorname{arctg}(c\Delta t k'). \tag{2.5}$$

The Crank–Nicholson scheme being more stable than the Leap–Frog scheme (see (1.15)), we can use a time step larger for the Crank–Nicholson scheme than for the Leap–Frog scheme. In Fig. 2(a), we have represented the ratio $c_{\mathrm{LF},k}/c$ and $c_{\mathrm{CN},k}/c$, using a time step five times larger for the Crank–Nicholson scheme (2.5) than for the Leap–Frog scheme (2.4). We can see the dispersive error, increasing with the high wavenumbers, due to the Crank–Nicholson scheme. So, the dispersive error, due to the Crank–Nicholson scheme, is more important on the small scales (large wavenumbers) than on the large ones (small wavenumbers). However, for the shallow water problem (1.5) considered here, the contribution of the small scales (large wavenumbers) on the solution (1.6) is small by comparison with that of the large scales (see [24]).

Let us now consider the time derivative of the solution (2.3); the modulus of the time derivative is $\mu_k = k'c|Q_k|$. If we consider, now, the modulus $\mu_{\mathrm{LF},k}$ (resp. $\mu_{\mathrm{CN},k}$) of the time derivative of the solution computed with the Leap–Frog scheme (2.4) (resp. Crank–Nicholson scheme (2.5)), we have $\mu_{\mathrm{LF},k} = k'c_{\mathrm{LF},k}|Q_k|$ (resp. $\mu_{\mathrm{CN},k} = k'c_{\mathrm{CN},k}|Q_k|$). In Fig. 2(b), we have represented the errors on the time derivative $\frac{|\mu_k-\mu_{\mathrm{LF},k}|}{\mu_k}$ and $\frac{|\mu_k-\mu_{\mathrm{CN},k}|}{\mu_k}$, due to the Leap–Frog and Crank–Nicholson schemes, as functions of the wavenumbers. We have assumed, for the dependence of $|Q_k|$ on k', that:

$$|Q_k| = (k')^{-3/2}, \tag{2.6}$$

which simulates the decrease of the kinetic energy spectrum (slope of $(k')^{-3}$ in the inertial range). We recall that we use a time step five times larger for the Crank–Nicholson scheme than for the Leap–Frog scheme. We can see, in Fig. 2(b), that the relative error on the time derivative, due to the Crank–Nicholson scheme, increases rapidly, even on the small wavenumbers. Moreover, this error is less important with the Leap–Frog scheme, especially on the small wavenumbers (small increasing). An error on the time derivative induces an error on the time evolution of the computed solution. We see, from (2.3) and (2.6), that the time derivative decreases in modulus when k' increases. So, the large (resp. small) scales are associated with the fast (resp. slow) time scales.

However, it is important to accurately compute the large scales (small wavenumbers), since the large scales are those which contain most of the kinetic energy and enstrophy (two-dimensional turbulent flows). Moreover, the large scales are associated with short time frequencies (large period in time), so spatial scale separation induces temporal scale separation (see [24]). It is on the small frequencies that the Coriolis force has a more important effect and, for atmospheric flows, the effect of the rotation of the earth is important (quasi-geostrophic flows, see [14]).

So, since:

- the explicit scheme (1.9) is more stable for the large scales than for the small ones (see (1.10)),
- the relative error on the time derivative due to the semi-implicit scheme (1.14) is more important on the large scales than that due to the explicit scheme (1.9),
- it is important to accurately compute the large scales of the flow (more accuracy is required on the large scales than on the small scales),

we can envision to adapt the time scheme used (explicit scheme (1.9) or semi-implicit scheme (1.14)) to the size of the scales computed, i.e., according to the size of the wavenumber k (multilevel scheme). However, this requires:

(i) to be able to separate the scales and to choose a cut-off level to define the small and large scales;
(ii) to choose a time step Δt function of the scale size, i.e., of the wavenumber k, or Δt being wavenumber independent, i.e., identical for all the scales;
(iii) to choose a time scheme function of k: the explicit scheme (1.9) for the small wavenumbers k (large scales), and the semi-implicit scheme (1.14) for the large wavenumbers k (small scales).

To define such a multilevel scheme, the first step (step (i)) is to separate the scales. For the spectral Galerkin method previously described in Section 1, this separation is quite natural. For the dependent variables, ω, δ and h, let us consider a cut-off level $N_1 < N$, $k_{N_1} = \frac{N_1}{2}$ being the cut-off wavenumber associated. To define and separate the small and large scales, we write:

$$\begin{aligned}
\omega_N(\mathbf{x},t) &= \omega_{N_1}(\mathbf{x},t) + \omega_{N_1}^N(\mathbf{x},t),\\
\delta_N(\mathbf{x},t) &= \delta_{N_1}(\mathbf{x},t) + \delta_{N_1}^N(\mathbf{x},t),\\
h_N(\mathbf{x},t) &= h_{N_1}(\mathbf{x},t) + h_{N_1}^N(\mathbf{x},t),
\end{aligned} \tag{2.7}$$

where ω_{N_1}, δ_{N_1} and h_{N_1} are associated with the large scales (small wavenumbers):

$$\begin{pmatrix} \omega_{N_1}(\mathbf{x},t)\\ \delta_{N_1}(\mathbf{x},t)\\ h_{N_1}(\mathbf{x},t)\end{pmatrix} = \sum_{\mathbf{k}\in\mathbb{I}_{N_1}} \begin{pmatrix} \hat{\omega}_{\mathbf{k}}(t)\\ \hat{\delta}_{\mathbf{k}}(t)\\ \hat{h}_{\mathbf{k}}(t)\end{pmatrix} \exp(\mathrm{i}\mathbf{k}'\cdot\mathbf{x}), \tag{2.8}$$

and $\omega_{N_1}^N$, $\delta_{N_1}^N$ and $h_{N_1}^N$ are associated with the small scales (large wavenumbers):

$$\begin{pmatrix} \omega_{N_1}^N(\mathbf{x},t)\\ \delta_{N_1}^N(\mathbf{x},t)\\ h_{N_1}^N(\mathbf{x},t)\end{pmatrix} = \sum_{\mathbf{k}\in\mathbb{I}_N\setminus\mathbb{I}_{N_1}} \begin{pmatrix} \hat{\omega}_{\mathbf{k}}(t)\\ \hat{\delta}_{\mathbf{k}}(t)\\ \hat{h}_{\mathbf{k}}(t)\end{pmatrix} \exp(\mathrm{i}\mathbf{k}'\cdot\mathbf{x}). \tag{2.9}$$

We can rewrite (2.8) and (2.9) using the projection operators:

$$w_{N_1} = P_{N_1} w \quad \text{and} \quad w_{N_1}^N = Q_{N_1}^N w, \tag{2.10}$$

where P_{N_1} and $Q_{N_1}^N$ are the orthogonal projections, in $L^2(\Omega)$, onto the spaces V_{N_1} and $V_N \setminus V_{N_1}$, respectively, and $w = \omega$, δ or h.

Remark 2.1. Considering several cut-off levels N_i and applying recursively the same scale separation on the small scales, we can define more than two levels of scales.

Now, we are looking for the equations associated with the time evolution of the large scales. To obtain these equations, we impose that the orthogonal projection of the residuals (obtained substituting ω_N, δ_N, h_N, to ω, δ and h in (1.5)), on the space V_{N_1}, are null (least square method).

Using the orthogonality properties of the trigonometric polynomials in $L^2(\Omega)$, we obtain the following system of ODEs, for the Fourier coefficients $\hat{\omega}_{\mathbf{k}}, \hat{\delta}_{\mathbf{k}}, \hat{h}_{\mathbf{k}}, \mathbf{k} \in \mathbb{I}_{N_1}$ (small wavenumbers, large scales):

$$\begin{aligned}
&\frac{\mathrm{d}}{\mathrm{d}t}\hat{\omega}_{\mathbf{k}} + \nu_{\mathrm{T}}|\mathbf{k}'|^{4p}\hat{\omega}_{\mathbf{k}} + P_{N_1}\widehat{(T_{\omega,N})}(\mathbf{k}) + f\hat{\delta}_{\mathbf{k}} = 0,\\
&\frac{\mathrm{d}}{\mathrm{d}t}\hat{\delta}_{\mathbf{k}} + \nu_{\mathrm{T}}|\mathbf{k}'|^{4p}\hat{\delta}_{\mathbf{k}} + P_{N_1}\widehat{(T_{\delta,N})}(\mathbf{k}) - f\hat{\omega}_{\mathbf{k}} - g|\mathbf{k}'|^2\hat{h}_{\mathbf{k}} = 0,\\
&\frac{\mathrm{d}}{\mathrm{d}t}\hat{h}_{\mathbf{k}} + \nu_{\mathrm{T}}|\mathbf{k}'|^{4p}\hat{h}_{\mathbf{k}} + H\hat{\delta}_{\mathbf{k}} + P_{N_1}\widehat{(T_{h,N})}(\mathbf{k}) = 0.
\end{aligned} \tag{2.11}$$

Similarly, to obtain the equations associated with the time evolution of the small scales, we use a least square method, i.e., we impose that the orthogonal projection of the residual on the space $V_N \setminus V_{N_1}$ is null. Using the orthogonality properties of the trigonometric polynomials in $L^2(\Omega)$, we obtain the following system of ODEs, for the Fourier coefficients $\hat{\omega}_{\mathbf{k}}, \hat{\delta}_{\mathbf{k}}, \hat{h}_{\mathbf{k}}, \mathbf{k} \in \mathbb{I}_N \setminus \mathbb{I}_{N_1}$ (large wavenumbers, small scales):

$$\begin{aligned}
&\frac{\mathrm{d}}{\mathrm{d}t}\hat{\omega}_{\mathbf{k}} + \nu_{\mathrm{T}}|\mathbf{k}'|^{4p}\hat{\omega}_{\mathbf{k}} + \widehat{Q_{N_1}^N(T_{\omega,N})}(\mathbf{k}) + f\hat{\delta}_{\mathbf{k}} = 0,\\
&\frac{\mathrm{d}}{\mathrm{d}t}\hat{\delta}_{\mathbf{k}} + \nu_{\mathrm{T}}|\mathbf{k}'|^{4p}\hat{\delta}_{\mathbf{k}} + \widehat{Q_{N_1}^N(T_{\delta,N})}(\mathbf{k}) - f\hat{\omega}_{\mathbf{k}} - g|\mathbf{k}'|^2\hat{h}_{\mathbf{k}} = 0,\\
&\frac{\mathrm{d}}{\mathrm{d}t}\hat{h}_{\mathbf{k}} + \nu_{\mathrm{T}}|\mathbf{k}'|^{4p}\hat{h}_{\mathbf{k}} + H\hat{\delta}_{\mathbf{k}} + \widehat{Q_{N_1}^N(T_{h,N})}(\mathbf{k}) = 0.
\end{aligned} \tag{2.12}$$

Remark 2.2. The orthogonal projections P_{N_1} and $Q_{N_1}^N$, defined in (2.10), commute with the partial derivative operators, because of the periodic boundary conditions (trigonometric polynomials are used as Galerkin basis). Hence the coupling between the large scales (see (2.11)) and the small scales (see (2.12)) is done through the nonlinear terms:

$$\begin{aligned}
T_{\omega,N} =& T_{\omega,N}(\mathbf{u}_{\mathbf{N}}, \omega_N) = T_{\omega,N}(\mathbf{u}_{\mathbf{N_1}} + \mathbf{u}_{\mathbf{N_1}}^{\mathbf{N}}, \omega_{N_1} + \omega_{N_1}^N)\\
=& T_{\omega,N}(\mathbf{u}_{\mathbf{N_1}}, \omega_{N_1}) + T_{\omega,N}(\mathbf{u}_{\mathbf{N_1}}, \omega_{N_1}^N) + T_{\omega,N}(\mathbf{u}_{\mathbf{N_1}}^{\mathbf{N}}, \omega_{N_1}) + T_{\omega,N}(\mathbf{u}_{\mathbf{N_1}}^{\mathbf{N}}, \omega_{N_1}^N),\\
T_{\delta,N} =& T_{\delta,N}(\mathbf{u}_{\mathbf{N}}, \omega_N) = T_{\delta,N}(\mathbf{u}_{\mathbf{N_1}} + \mathbf{u}_{\mathbf{N_1}}^{\mathbf{N}}, \omega_{N_1} + \omega_{N_1}^N)\\
=& T_{\delta,N}(\mathbf{u}_{\mathbf{N_1}}, \omega_{N_1}) + T_{\delta,N}(\mathbf{u}_{\mathbf{N_1}}, \omega_{N_1}^N) + T_{\delta,N}(\mathbf{u}_{\mathbf{N_1}}^{\mathbf{N}}, \omega_{N_1}) + T_{\delta,N}(\mathbf{u}_{\mathbf{N_1}}^{\mathbf{N}}, \omega_{N_1}^N),\\
T_{h,N} =& T_{h,N}(\mathbf{u}_{\mathbf{N}}, h_N) = T_{h,N}(\mathbf{u}_{\mathbf{N_1}} + \mathbf{u}_{\mathbf{N_1}}^{\mathbf{N}}, h_{N_1} + h_{N_1}^N)\\
=& T_{h,N}(\mathbf{u}_{\mathbf{N_1}}, h_{N_1}) + T_{h,N}(\mathbf{u}_{\mathbf{N_1}}, h_{N_1}^N) + T_{h,N}(\mathbf{u}_{\mathbf{N_1}}^{\mathbf{N}}, h_{N_1}) + T_{h,N}(\mathbf{u}_{\mathbf{N_1}}^{\mathbf{N}}, h_{N_1}^N).
\end{aligned} \tag{2.13}$$

Now, we want to define a cut-off level $N_1 < N$ to separate the small and large scales. As it has been previously said (see step (iii)), the aim is to apply the explicit scheme (1.9) on the large scales (small wavenumbers) and the semi-implicit scheme (1.14) on the small scales (large wavenumbers). Let us denote by Δt_{e} the time step used for the explicit scheme (i.e., for the small wavenumbers), and by Δt_{i} the time step used for the semi-implicit scheme (i.e., for the large wavenumbers). We suppose that we have chosen the time step Δt_{e}. Using the stability constraint (1.10) associated with the explicit scheme (1.9), we define a cut-off wavenumber $k'_{N_1} = \frac{2\pi}{L_x} k_{N_1} = \sqrt{2}\frac{2\pi}{L_x}\frac{N_1}{2}$, such that the explicit scheme is stable for the choice of Δt_{e} and for $k \leqslant k_{N_1}$ (large scales), and unstable for $k > k_{N_1}$ (small scales). If this cut-off level N_1 is too low, we must decrease the time step Δt_{e} chosen.

Now, we shall consider the second step previously defined (step (ii)). We shall present different strategies for the time integration of the small and large scales, leading to different multilevel methods. For all these multilevel methods, we used the explicit scheme (1.9) to compute the large scales (corresponding to $0 \leqslant k' \leqslant k'_{N_1}$), with the time step Δt_{e}, and the semi-implicit scheme (1.14) to compute the small scales (corresponding to $k'_{N_1} < k' \leqslant k'_N$), with the time step Δt_{i}. We denote by Δt_{Ref} the time step retained in Section 3.1 for the reference simulation, i.e., for the simulation corresponding to the explicit scheme (1.9) used to compute all the scales $0 \leqslant k' \leqslant k'_N$ (explicit reference scheme). As we shall see later, such a simulation will be used as the reference simulation to compare the numerical results obtained with the new proposed schemes (see Sections 3 and 5). The different multilevel schemes now proposed are based on different choices for the time steps Δt_{e} and Δt_{i} used for the explicit and semi-implicit schemes, respectively.

2.1. Scheme S_1

In this case, we choose $\Delta t_e = \Delta t_i > \Delta t_{Ref}$, since the explicit time scheme is used only for the large scales, and it is more stable for the small wavenumbers.

The drawback, of such a scheme, is that it does not allow to choose a time step much larger than Δt_{Ref}, otherwise the cut-off level N_1 is too low, and we retrieve approximately the semi-implicit scheme (1.14) on all the wavenumbers k', i.e., to compute all the scales.

The numerical results, obtained with this scheme, will be presented in Section 3.3.

2.2. Scheme S_2

In order to overcome the drawback of the numerical stability problem previously explained when $\Delta t_e = \Delta t_i$ (see Scheme S_1), we choose here $\Delta t_i > \Delta t_e$. For example, we choose $\Delta t_e = \Delta t_{Ref}$ and $\Delta t_i = l\Delta t_{Ref}$, with $l > 1$. Such a choice induces a closure problem, since $\Delta t_i > \Delta t_e$. Indeed, the computation of the large scales $\omega_{N_1}^{n+1}$, $\delta_{N_1}^{n+1}$ and $h_{N_1}^{n+1}$ requires to know the small scales $\omega_{N_1}^{N}$, $\delta_{N_1}^{N}$ and $h_{N_1}^{N}$ at the previous time. This is due to the nonlinear terms coupling the large and small scales (see (2.13)). The closure is obtained in the following manner: since the stability constraint (CFL condition) $Stab_1$, defined in (1.11) and due to the explicit treatment of the nonlinear terms, is not the most restrictive one (the most restrictive one being $Stab_3$, defined in (1.13), and due to the explicit treatment of the gravity terms), we will retain the values of the nonlinear coupling terms in (2.11), i.e., $(P_{N_1}(T_{q,N}(\mathbf{u}_{\mathbf{N_1}}, \omega_{N_1}^N)) + P_{N_1}(T_{q,N}(\mathbf{u}_{\mathbf{N_1}}^{\mathbf{N}}, \omega_{N_1}))) + P_{N_1}(T_{q,N}(\mathbf{u}_{\mathbf{N_1}}^{\mathbf{N}}, \omega_{N_1}^N))$ with $q = \omega$ or δ that is the vorticity or the plane divergence equation, and $P_{N_1}(T_{h,N}(\mathbf{u}_{\mathbf{N_1}}, h_{N_1}^N)) + P_{N_1}(T_{h,N}(\mathbf{u}_{\mathbf{N_1}}^{\mathbf{N}}, h_{N_1})) + P_{N_1}(T_{h,N}(\mathbf{u}_{\mathbf{N_1}}^{\mathbf{N}}, h_{N_1}^N))$ in the height equation, at the time $t_n = n\Delta t$, during the l time steps $t_{n+i} = (n+i)\Delta t$, $i = 1, \ldots, l$, for the computation of the large scales (quasi-static approximation, see [15–17]). For example, for $l = 5$, we compute the large scales with the explicit scheme (1.9) at the times t_n, $t_{n+1}, \ldots, t_{n+5}$ with the time step $\Delta t_e = \Delta t_{Ref}$, and we compute the small scales with the semi-implicit scheme

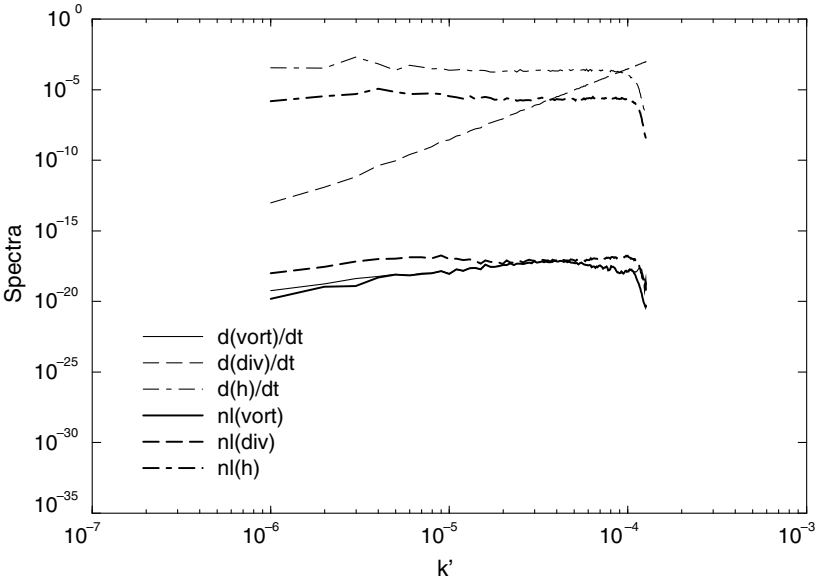

Fig. 3. Spectra of time derivatives (thin lines) and nonlinear terms (thick lines) for the vorticity (solid lines), plane divergence (dashed lines) and height (dot-dashed lines) equations of the shallow water problem.

(1.14) at the times t_n and t_{n+5} with the time step $\Delta t_i = 5\Delta t_{\mathrm{Ref}}$. In this way, it is necessary to only compute the nonlinear terms $P_{N_1}(T_{\omega,N}(\mathbf{u}_{\mathbf{N_1}}, \omega_{N_1})) = T_{\omega,N_1}(\mathbf{u}_{\mathbf{N_1}}, \omega_{N_1}), P_{N_1}(T_{\delta,N}(\mathbf{u}_{\mathbf{N_1}}, \omega_{N_1})) = T_{\delta,N_1}(\mathbf{u}_{\mathbf{N_1}}, \omega_{N_1})$ and $P_{N_1}(T_{h,N}(\mathbf{u}_{\mathbf{N_1}}, h_{N_1})) = T_{h,N_1}(\mathbf{u}_{\mathbf{N_1}}, h_{N_1})$, which are estimated on the coarse cut-off level $N_1 < N$, at the times t_{n+i}, $i = 1, \ldots, l-1$, inducing a saving in CPU time: $O(N_1^2 \log_2(N_1))$ operations instead of $O(N^2 \log_2(N))$ at the times t_{n+i}, $i = 1, \ldots, l-1$. Here, the quasi-static approximation not induces lost of accuracy since the nonlinear terms are not dominant in the shallow water problem (1.5) as we see in Fig. 3 (see, also [46]). Note that this may not always be the case for the shallow water equations, high speed flows over steep topography is an example of a situation in which the quasi-static approximation may be invalid.

The numerical results, obtained with this scheme, are presented in Section 3.4.

Remark 2.3. Consider, for example, the nonlinear term $P_{N_1}(T_{\omega,N}(\mathbf{u}_{\mathbf{N_1}}, \omega_{N_1})) = T_{\omega,N_1}(\mathbf{u}_{\mathbf{N_1}}, \omega_{N_1})$. In fact, we have $P_{N_1}(T_{\omega,N}(\mathbf{u}_{\mathbf{N_1}}, \omega_{N_1})) \simeq T_{\omega,N_1}(\mathbf{u}_{\mathbf{N_1}}, \omega_{N_1})$ instead of an equality, as it has been previously written. However, the difference is the aliasing error and, since we use the 3/2 rule to eliminate it, we recover an equality. This remark is also true for the nonlinear terms $P_{N_1}(T_{\delta,N}(\mathbf{u}_{\mathbf{N_1}}, \omega_{N_1})) = T_{\delta,N_1}(\mathbf{u}_{\mathbf{N_1}}, \omega_{N_1})$ and $P_{N_1}(T_{h,N}(\mathbf{u}_{\mathbf{N_1}}, h_{N_1})) = T_{h,N_1}(\mathbf{u}_{\mathbf{N_1}}, h_{N_1})$.

3. Numerical results (multilevel methods)

We shall present, in this section, the numerical results obtained with the explicit reference scheme (1.9) used to compute all the scales, with the semi-implicit scheme (1.14) used to compute all the scales, and with the two new multilevel schemes S_1 and S_2 described in Section 2.

The aim is to obtain new schemes to resolve the shallow water problem (1.5), with better stability properties than the explicit scheme (1.9), in order to increase the time step and, so, to reduce the CPU time used, avoiding a too large dispersive error. Ideally we want, through the new proposed schemes, to be able to compute the numerical solution of (1.5), with approximately the accuracy of the explicit scheme (1.9), and with nearly the time step (and so the CPU time) of the semi-implicit scheme (1.14).

3.1. Explicit reference scheme

Now, we are going to present the numerical results obtained with the explicit scheme (1.9). This scheme is used as a reference, in order to compare the results obtained with the semi-implicit scheme (1.14) and with the new proposed schemes, since less dispersive error appears with this explicit scheme, than with the semi-implicit scheme (1.14) when the time step is increased.

We choose $H = 10^4$ m (troposphere) and $N = 256$. The size of the smallest scales which are computed, i.e., the mesh size, is $L_x/N \simeq 25$ km. To model the action of the small scales, not taken into account in the computation, we use the hyperdissipative operator defined in (1.3), with $p = 2$ as the turbulence model. For the eddy viscosity ν_T defined in (1.4), we have retained $\zeta = 10^4$. As we can see in Fig. 4(a), we well recover an energy spectrum with a k'^{-3} slope (see Section 1), evidencing a good behavior of the eddy viscosity model to dissipate energy in the inertial range, dissipation due to the small scales not computed and modeled with the turbulence model. The slope of the height spectrum in Fig. 4(a) is indeed in k'^{-5} (see Section 1).

The time step retained in order to obtain the numerical stability is $\Delta t_{\mathrm{Ref}} = 10$ s. In this way the stability constraint $Stab_3$, defined in (1.13), is approximatively equal to one. We can notice that if we choose $\Delta t_{\mathrm{Ref}} = 20$ s, the explicit scheme is unstable and we quickly obtain an overflow in the numerical simulations.

For $N = 256$, the required CPU time on one processor of an IBM SP is 1.44 s for one time step. The choice of the initial condition is obtained firstly by imposing an energy spectrum decreasing as k'^{-3}

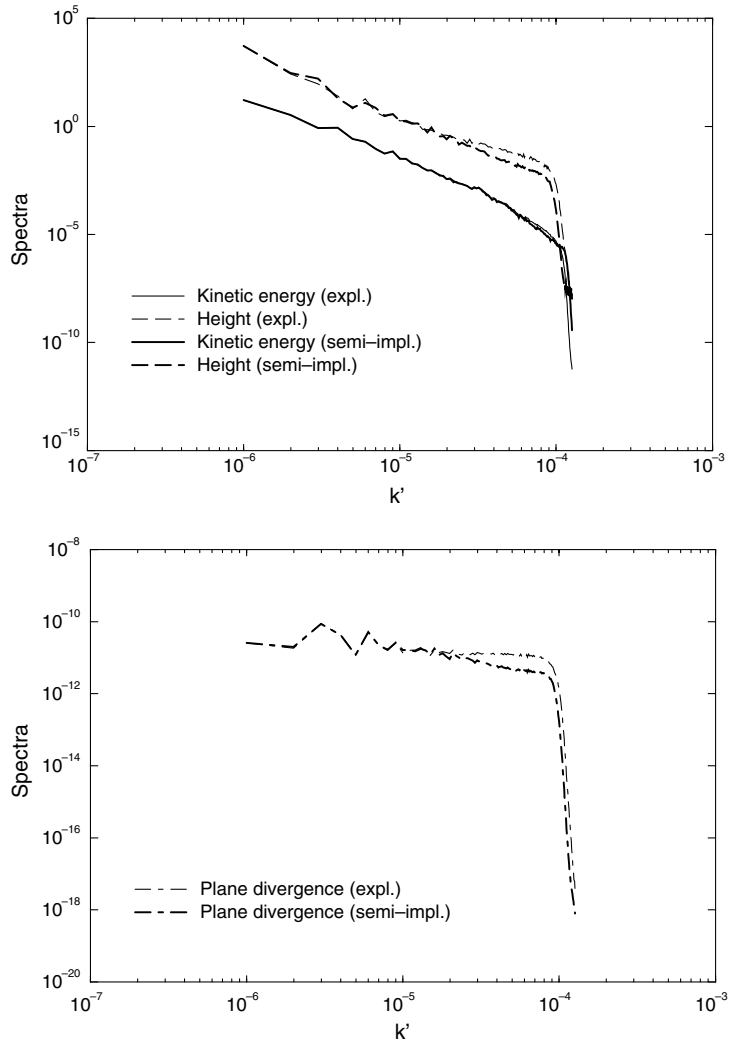

Fig. 4. Spectra of velocity (kinetic energy spectrum), height and plane divergence for the explicit reference scheme (thin lines) and for the semi-implicit scheme (thick lines). The semi-implicit scheme corresponds to the choice of $\Delta t = 50$ s.

(two-dimensional turbulent flow), and with a plane divergence δ equal to zero (barotropic flow). We run some time iterations until reaching a statistically steady state, i.e., the time average of global quantities in space are approximately time independent. Then, we use this velocity field to start the comparison between the new proposed schemes and the reference explicit scheme. For more details, see [15]. Since the explicit Leap–Frog scheme required two initial time steps, the first time step is obtained using an explicit third order Runge–Kutta scheme. The comparison is done over 20 days (namely 176,000 time steps for the explicit reference scheme).

As in turbulence modeling, we look for the large scales of the flow since those are the scales which contain the kinetic energy and the enstrophy in two-dimensional turbulent flows. So we look at such global quantities, characteristic of turbulent flows. More precisely, in order to compare the different schemes described here, we compute some global quantities in space, such as spectra: energy spectrum, spectrum

of the height, spectrum of the divergence, to obtain a scale comparison according to the scale decomposition of the computed variables. In the same manner, we compute some physical characteristic quantities, such as the kinetic energy $\|\mathbf{u}\|_{L^2(\Omega)}$ (or energy norm of the velocity field):

$$\|\mathbf{u}\|^2_{L^2(\Omega)} = \int_\Omega |\mathbf{u}(\mathbf{x})|^2 \, d\mathbf{x},$$

the enstrophy $\|\mathbf{u}\|_{H^1(\Omega)}$ (or enstrophy norm, i.e., energy norm of the gradient of the velocity field):

$$\|\mathbf{u}\|^2_{H^1(\Omega)} = \int_\Omega |\nabla \mathbf{u}(\mathbf{x})|^2 \, d\mathbf{x},$$

and the maximum value of the velocity $\|\mathbf{u}\|_{L^\infty(\Omega)}$:

$$\|\mathbf{u}\|_{L^\infty(\Omega)} = \sup_\Omega |\mathbf{u}(\mathbf{x})|.$$

Moreover, in order to compare the computed dependent variables ω, δ and h, we compare the energy norm of the vorticity ω, of the plane divergence δ and of the height h.

Most of the CPU time is used for the computation of the nonlinear terms, which requires, at each time step, 9 FFT, so around $9(N^2 \log_2(N))$ operations (see Section 1), with $N = 256$. Let us denote by Nb_{Ref} the total number of operations required for the explicit scheme over 20 days of simulation (namely 176,000 time steps), that is $Nb_{\mathrm{Ref}} \simeq 9(N^2 \log_2(N)) \times 176{,}000$ operations.

At the initial time we have imposed that the plane divergence $\delta = 0$. The Rossby and the Froude numbers for the simulation considered here are:

$$Ro = \frac{U}{fL} \text{ (comparison of the advection effect with the rotation effect)},$$
$$Fr = \frac{U}{\sqrt{gH}} \text{ (comparison of the advection effect with the gravity effect)},$$

where U is a characteristic velocity and L a characteristic horizontal length.

In Fig. 5(a), we have represented the energy norm of the velocity field computed with the explicit reference scheme. We have $\|\mathbf{u}\|_{L^2(\Omega)} \simeq 23.5$. So, we choose $U = 23.5$ as a characteristic velocity and we have:

$$Ro = \frac{23.5}{10^{-4} \times 6.31 \times 10^6} \simeq 3.7 \times 10^{-2} \ll 1,$$

and:

$$Fr = \frac{23.5}{\sqrt{9.81 \times 10^4}} \simeq 7.5 \times 10^{-2} \ll 1.$$

Since $Fr \simeq Ro \ll 1$, the computed flow is quasi-geostrophic. Moreover, the aspect ratio:

$$\frac{H}{L} = \frac{10^4}{6.31 \times 10^6} = 1.6 \times 10^{-3}$$

is quite small. Since Ro and Fr are small, we conclude that the advection effect, associated with the nonlinear terms, is small by comparison with the rotation and gravity effects (see Fig. 3). This has been used for the S_2 scheme (see Section 2.2).

The effect of the Coriolis force being the stratification of the flow (see [14]), and this effect being important by comparison with advection ($Ro \ll 1$), the vertical component of the velocity is small. So, due to the incompressibility of the fluid, the plane divergence δ is small also, and the height of the free surface h is

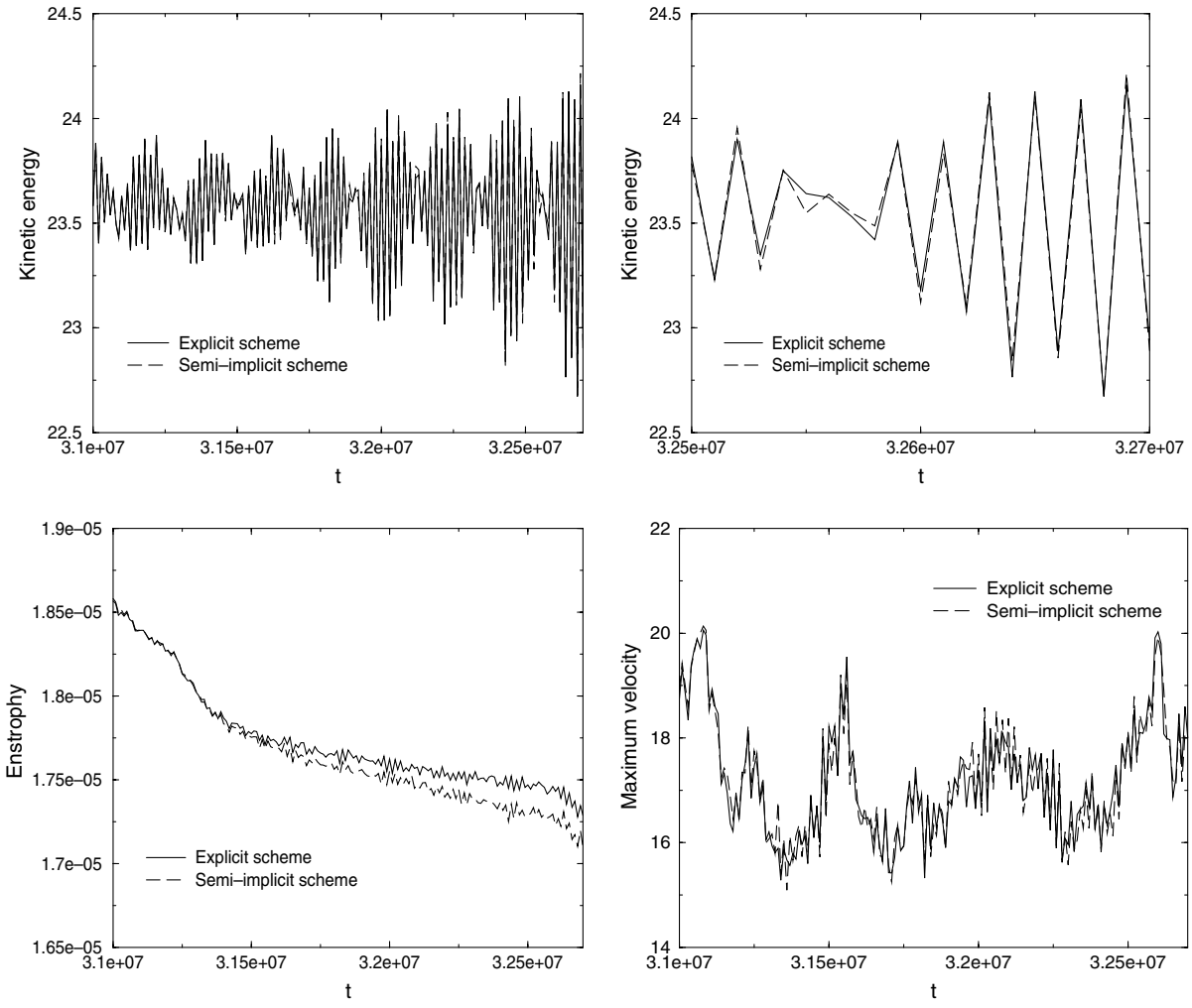

Fig. 5. Representation of the kinetic energy, the enstrophy, and the maximum velocity as functions of t. The semi-implicit scheme corresponds to the choice of $\Delta t = 50$ s.

small, by comparison with the mean height H, in agreement with the numerical results obtained (see Section 3.2).

3.2. Semi-implicit scheme

For the same choice of the parameters, but using the semi-implicit scheme (1.14) instead of the explicit scheme (1.9), we have retained $\Delta t = 50\text{ s} = l\Delta t_{\text{Ref}}$, with $l = 5$. With this choice, the semi-implicit scheme is stable. We notice that for a choice of the parameter l larger than 5, the semi-implicit scheme (1.14) is still stable, but the difference with the explicit (reference) scheme (1.9) is increased.

The complexity of the computation is, approximately, of the same order for the explicit and for the semi-implicit schemes, on one time step. In particular, one time step requires the same number of FFTs to compute the nonlinear terms, for which the essential part of the CPU time is used. So, if we denote

by Nb_i the total number of operations required for the semi-implicit scheme over 20 days of simulation (i.e., 35,200 time steps), we have $Nb_i = \frac{Nb_{\mathrm{Ref}}}{5} = 20\% Nb_{\mathrm{Ref}}$.

In Figs. 4–6, we have compared the quantities computed with the explicit reference scheme and with the semi-implicit scheme.

In Fig. 4, we have represented the spectra associated with the velocity (kinetic energy spectrum), the height and the plane divergence. As we can see, the spectra are quite similar. Some differences appear on the height spectrum, even for the low wavenumbers (large scale), but the slope of the spectrum is preserved.

Then we consider, in Fig. 5, the kinetic energy $\|\mathbf{u}\|_{L^2(\Omega)}$ (see Figs. 5(a) and (b)), the enstrophy $\|\mathbf{u}\|_{H^1(\Omega)}$ (see Fig. 5(c)) and the maximum velocity $\|\mathbf{u}\|_{L^\infty(\Omega)}$ (see Fig. 5(d)), computed with the explicit and with the semi-implicit schemes. As we can see in Figs. 5(a) and (b), a decorrelation of the curves associated with the explicit scheme and with the semi-implicit scheme appears from time to time. Moreover, when the time increases, the amplitude of the decorrelation and the width of the period of the decorrelation increase.

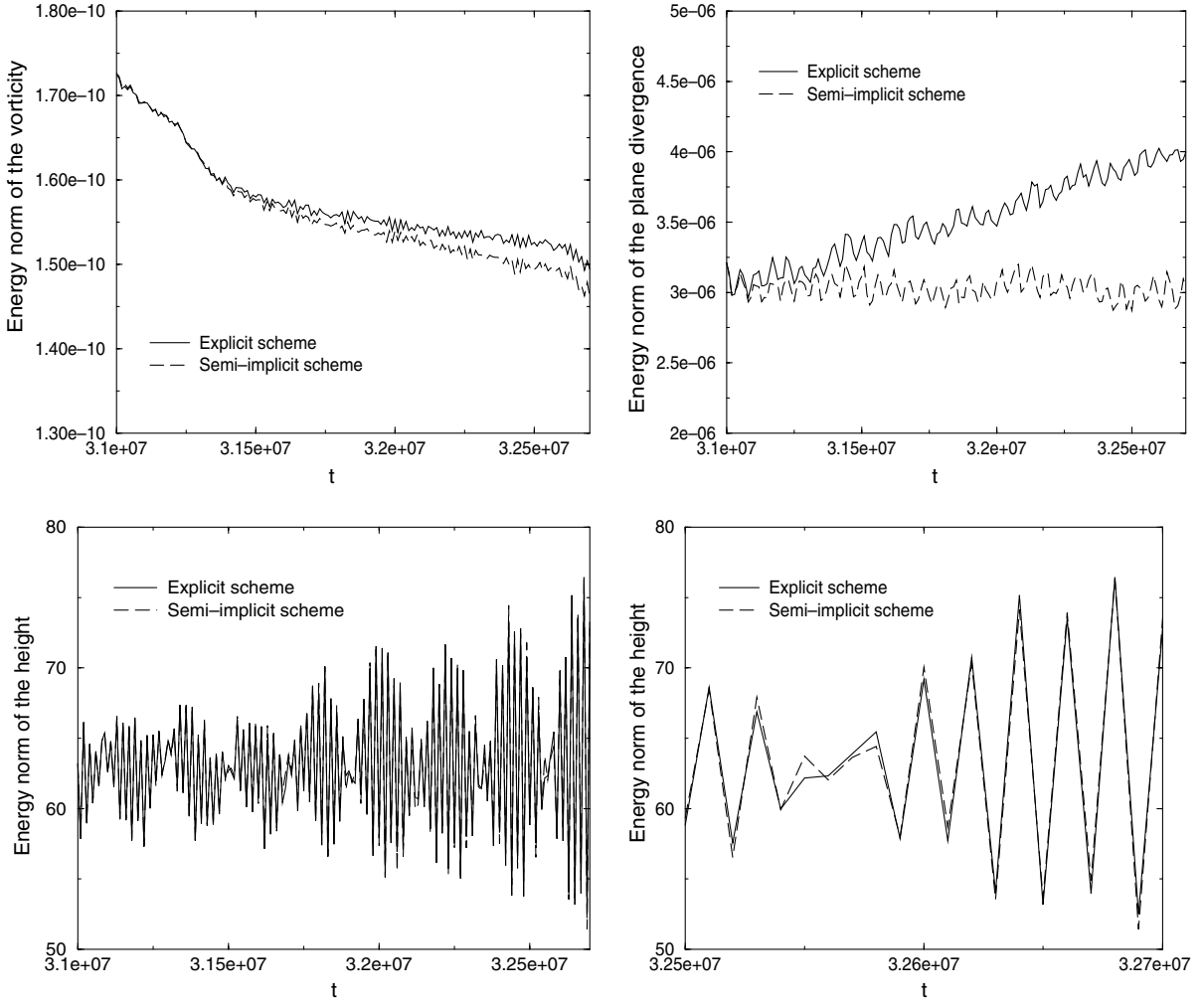

Fig. 6. Representation of the energy norm of the vorticity ω, of the plane divergence δ, and of the height h as functions of t. The semi-implicit scheme corresponds to the choice of $\Delta t = 50$ s.

For the enstrophy, the value is small, since there is a small energy dissipation rate (fluid with no kinetic viscosity). The slow decrease of the enstrophy with time, due to the turbulence model, is quite similar for the explicit and semi-implicit schemes.

As for the maximum velocity (L_∞ norm), the average profile of the time evolution is quite similar for the two schemes, even though the oscillations around this profile are different.

In Fig. 6, we have represented the energy norm of the vorticity ω (see Fig. 6(a)), of the plane divergence δ (see Fig. 6(b)) and of the height h (see Figs. 6(c) and (d)). The behavior of the vorticity, in time, is similar with the enstrophy (see Fig. 5(c)). For the plane divergence, the values are small, for all t, since atmospheric flows are quasi-geostrophic. Like in Fig. 5(d) (maximum velocity), the average profiles are quite similar, but some differences appear on the oscillations (high frequencies) around the average profile (low frequencies).

The height variable h is a characteristic quantity of the shallow water problem. As we can see in Figs. 6(c) and (d), we have a behavior similar to the kinetic energy (see Figs. 5(a) and (b)), with an increase of the width of the decorrelation period and of the amplitude oscillations obtained with the semi-implicit scheme, when t increases.

In summary, the differences between the explicit scheme and the semi-implicit scheme, due to the dispersive error of the semi-implicit scheme (see Section 1), appear essentially on the kinetic energy $\|\mathbf{u}\|_{L^2(\Omega)}$, and on the energy norm of the height $\|h\|_{L^2(\Omega)}$.

Now, if we consider the time averages of the relative errors between the explicit and semi-implicit schemes, the relative error on the kinetic energy $\|\mathbf{u}\|_{L^2(\Omega)}$ is around 5.0×10^{-4}, and the relative error on the energy norm of the height $\|h\|_{L^2(\Omega)}$ is approximately 6.1×10^{-3}, over the 20 days of the numerical comparisons (see Table 1).

Remark 3.1. The interest of the semi-implicit scheme is to allow to consider time steps larger than for the explicit scheme. However, if we choose for the semi-implicit scheme the same little time step as for the explicit scheme, we obtain results similar with the two schemes, due to the convergence of the schemes toward the exact solution. However, the explicit scheme is the proper reference state for the designed multilevel schemes. Indeed, the Crank–Nicholson scheme has half of the truncation error (and opposite sign) than the Leap–Frog scheme. However, this concerns only the standard two-time level Crank–Nicholson. The way how the semi-implicit algorithm is built here employs the trapezoidal integral over double time step, whereupon the resulting Crank–Nicholson scheme has twice larger truncation error than the standard leapfrog. Alternatively, one might consider the trapezoidal rule composed over two time steps $0.25(\psi^{n+1} + 2\psi^n + \psi^{n-1})$ for the gravity wave terms. Such a scheme would have formally the same size of the truncation error than the explicit scheme, but still the opposite sign.

3.3. Scheme S_1

Now, we want to compare the scheme S_1 (see Section 2.1) with the explicit reference scheme (1.9). We have retained $\Delta t_e = \Delta t_i = 5\Delta t_{Ref} = 50$ s. The cut-off level $N_1 < N$ is equal to $N_1 = 64$. In this way, the percentage of the Fourier coefficients computed with the explicit scheme over the total number of coefficients

Table 1
Relative errors in energy norm for the different schemes

	Semi-implicit $\Delta t = 50$ s	Semi-implicit $\Delta t = 30$ s	S_1	S_2	S_3
Velocity $\times 10^{-4}$	5.0	2.2	2.7	0.9	3.3
Height $\times 10^{-3}$	6.1	2.7	3.3	1.0	2.6

is around 5%. Notice that, this cut-off level is the highest cut-off level N_1 acceptable, to guarantee stability for the time step retained.

In Fig. 7, we consider the spectra for the velocity, the height and the plane divergence. The spectra obtained with the S_1 scheme are quite similar to the spectra obtained with the explicit reference scheme. Moreover, the low parts of the spectra are better described than with the semi-implicit scheme (see Fig. 4), especially for the kinetic energy spectrum.

Now, we consider, in Fig. 8, the kinetic energy (see Figs. 8(a) and (b)), the enstrophy (see Fig. 8(c)), and the maximum velocity (see Fig. 8(d)), computed with the explicit scheme and with the S_1 scheme. As we can see, the results are quite similar with those obtained for the semi-implicit scheme (see Fig. 5). However, for the kinetic energy i.e., $\|\mathbf{u}\|_{L^2(\Omega)}$, the retranscription is better with the S_1 scheme than with the semi-implicit scheme. Indeed, if we compare Figs. 8(a) and (b) with Figs. 5(a) and (b), we can see that the correlation

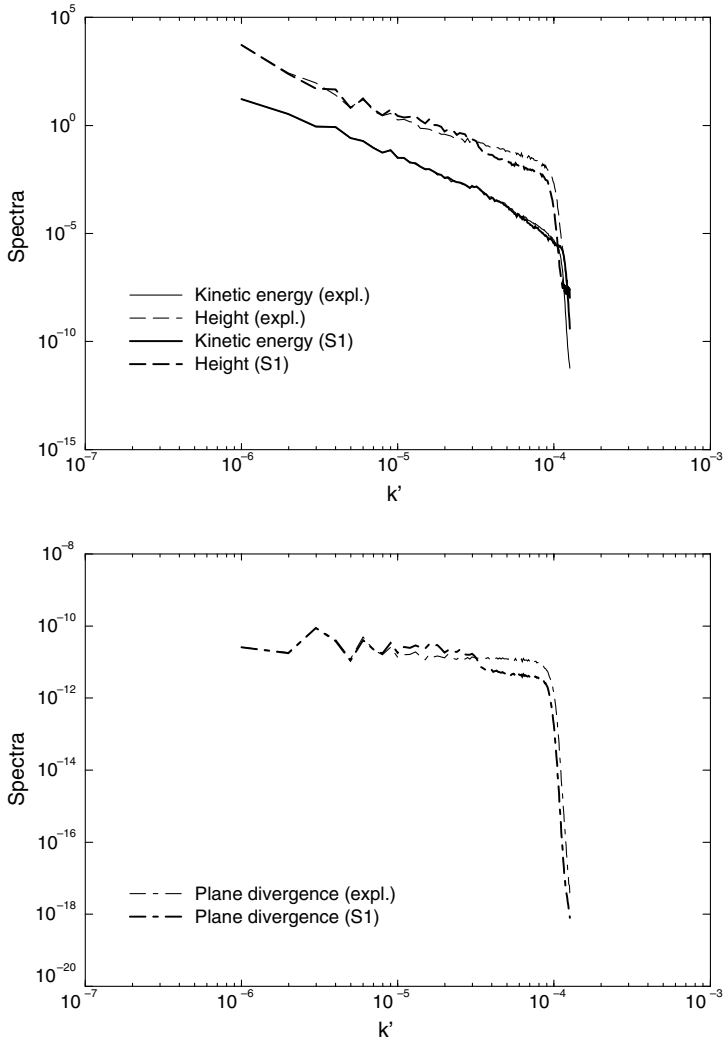

Fig. 7. Spectra of velocity (kinetic energy spectrum), height and plane divergence for the explicit reference scheme (thin lines) and for the scheme S_1 (thick lines).

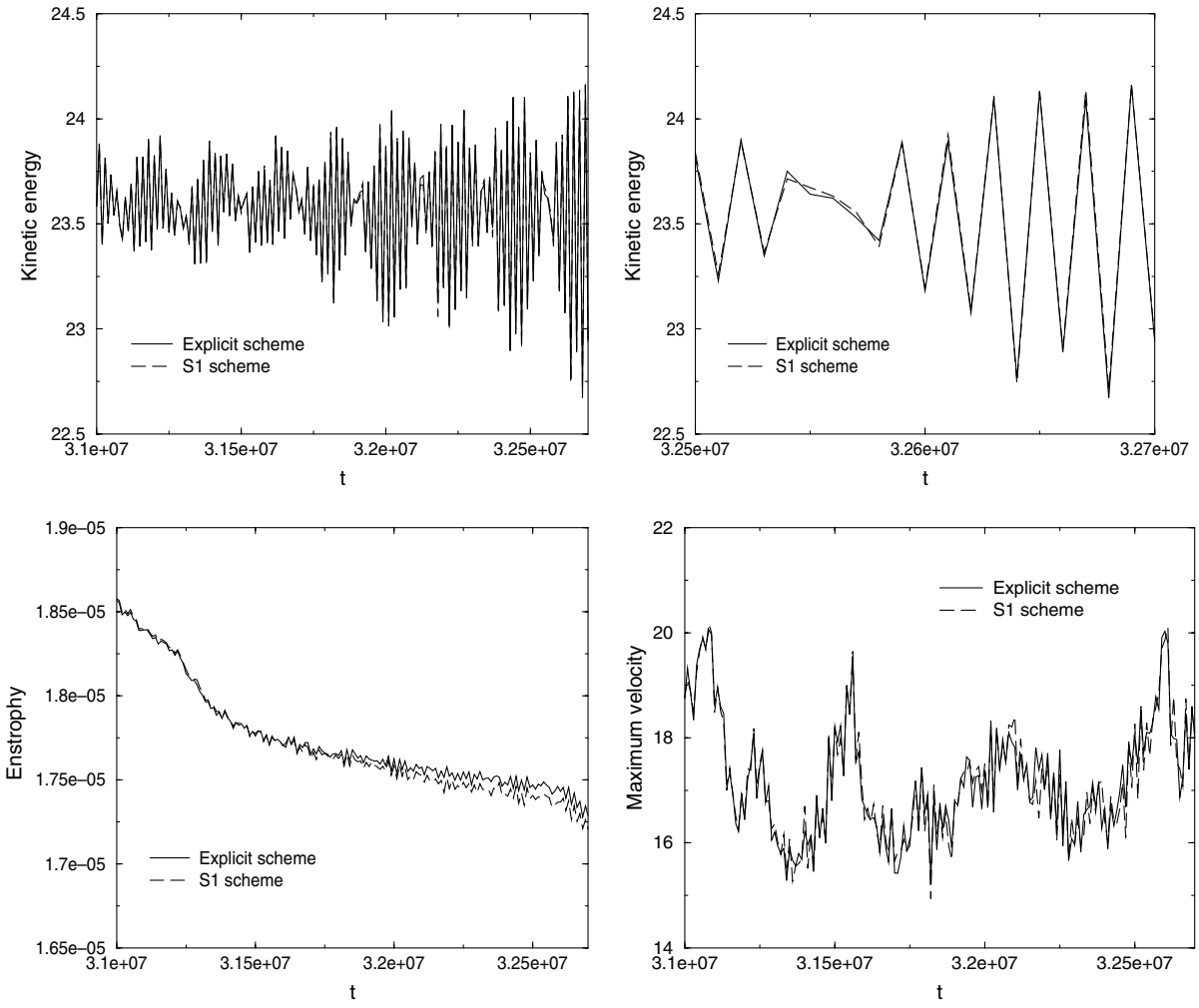

Fig. 8. Representation of the kinetic energy, the enstrophy, and the maximum velocity as functions of t.

between the curves of the explicit and S_1 schemes is better than for the explicit and semi-implicit schemes. In particular, there is no decorrelation of the curves when t increases, as it is the case in Fig. 5.

In Fig. 9, we have represented the energy norm of the vorticity ω (see Fig. 9(a)), of the plane divergence δ (see Fig. 9(b)), and of the height h (see Figs. 9(c) and (d)). Still here, we can see that the results of the comparison, with the explicit reference scheme, are quite similar with those obtained for the semi-implicit scheme (see Fig. 6), even if the plane divergence is slightly over estimated by comparison with the explicit scheme. However, as for the kinetic energy in Figs. 8(a) and (b), the correlation between the curves of the explicit and S_1 schemes, for the energy norm of the height, is better than for the explicit and semi-implicit schemes (see Figs. 9(c) and (d) and Figs. 6(c) and (d)). Moreover, there is no increase of the decorrelation when t increases.

If we consider the time averages of the relative errors between the explicit and S_1 schemes, the relative error on the kinetic energy $\|\mathbf{u}\|_{L^2(\Omega)}$ is around 2.7×10^{-4}, and that on the energy norm of the height $\|h\|_{L^2(\Omega)}$ is approximately equal to 3.3×10^{-3}, over the 20 days of the numerical comparisons (see Table 1).

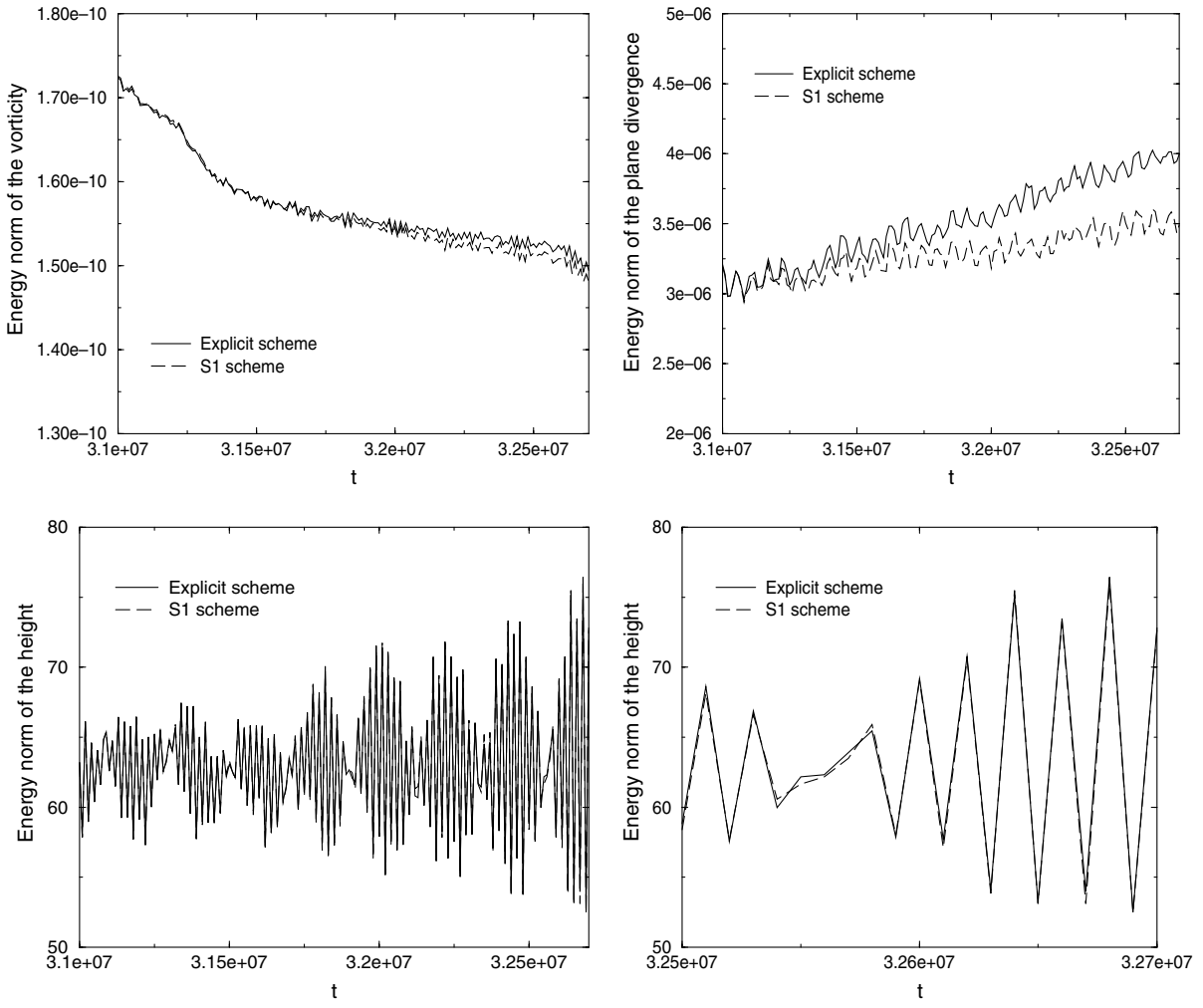

Fig. 9. Representation of the energy norm of the vorticity ω, of the plane divergence δ, and of the height h as functions of t.

Finally, the total number of operations Nb_{S_1} required for the S_1 scheme, over 20 days of simulation (i.e., 35,200 time steps), is approximately the same as for the semi-implicit scheme, namely Nb_i (see Section 3.2).

3.4. Scheme S_2

Finally, we want to compare the S_2 scheme (see Section 2.2) with the explicit reference scheme (1.9). We have chosen $\Delta t_e = \Delta t_{Ref} = 10$ s, and $\Delta t_i = 5\Delta t_{Ref} = 50$ s $> \Delta t_e$. The coarse level $N_1 < N$ is equal to $N_1 = N/2$. The total number of operations Nb_{S_2} required for the S_2 scheme, over the 20 days of simulation (i.e., 176,000 time steps), is larger than for the semi-implicit and S_1, but less than for the explicit reference scheme. Indeed, the evaluation of the nonlinear terms requires the computation of the FFT on the finest grid (i.e., $O(N^2 \log_2(N))$ operations) only once every five time steps and, for the other time steps, the nonlinear terms are estimated on the coarse level N_1, requiring FFT with $O(N_1^2 \log_2(N_1))$ operations, the coupling nonlinear terms being estimated with a quasi-static approximation (see Section 2.2). So, over $l = 5$

time steps, the number of operations required for the S_2 scheme is $(l-1)\times 9\times N_1^2\log_2(N_1)+9\times N^2\log_2(N)$ operations, instead of $l\times 9\times N^2\log_2(N)$ operations for the explicit scheme. For $l=5$, $N=256$ and $N_1=128$, the ratio of the number of operations required for the S_2 scheme on five time steps, over the number required for the explicit reference scheme on five time steps, is around 37%.

The total number of operations Nb_{S_2} required for the S_2 scheme, over 20 days of simulation (i.e., 176,000 time steps), is $Nb_{S_2}=35,200\times((l-1)\times 9\times N_1^2\log_2(N_1)+9\times N^2\log_2(N))\simeq 37\%Nb_{\mathrm{Ref}}$. So, Nb_{S_2} is around $0.37Nb_{\mathrm{Ref}}$, and $1.8Nb_{\mathrm{i}}$.

In Fig. 10, we have represented the spectra of the velocity field, of the height and of the plane divergence. The spectra obtained with the S_2 scheme are quite similar with those corresponding to the explicit scheme, especially for the low and medium ranges of the spectra, showing a better behavior of the S_2 scheme than the semi-implicit and S_1 schemes (see Figs. 4 and 7).

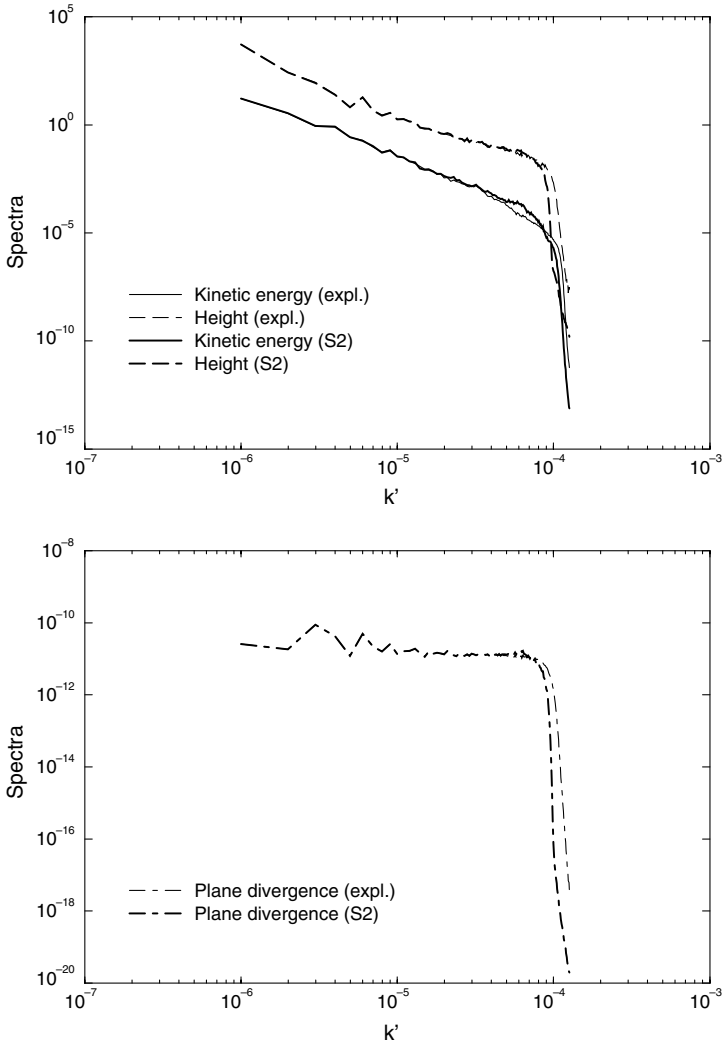

Fig. 10. Spectra of velocity (kinetic energy spectrum), height and plane divergence for the explicit reference scheme (thin lines) and for the scheme S_2 (thick lines).

Now, we consider, in Fig. 11, the kinetic energy (see Figs. 11(a) and (b)), the enstrophy (see Fig. 11(c)) and the maximum velocity (see Fig. 11(d)), computed with the explicit reference scheme and with the S_2 scheme. As we can see, the results obtained for the kinetic energy are quite similar with those obtained with the explicit reference scheme; and they are thus better than with the semi-implicit and S_1 schemes (see Figs. 5 and 8). For the kinetic energy, the curves are quite similar in phase and in amplitude. For the enstrophy, the differences with the explicit scheme appear much larger than for the semi-implicit and S_1 schemes (see Figs. 5(c) and 8(c)). However, the time average values are near 1.8×10^{-5}. The lesser decrease of the enstrophy obtained with the S_2 scheme, when the time increases, by comparison with the explicit scheme is due to the small increase of the velocity Fourier coefficients associated with the highest wavenumbers (see energy spectrum in Fig. 10), probably due to a modification of the action of the turbulence model (1.3) on the highest modes, since $\Delta t_i > \Delta t_e$ for the semi-implicit scheme applied on the high wavenumbers $|\mathbf{k}| > \frac{N_1}{2}$. As for the maximum velocity in Fig. 11(d), the average profiles (low frequencies) of the time evolution obtained

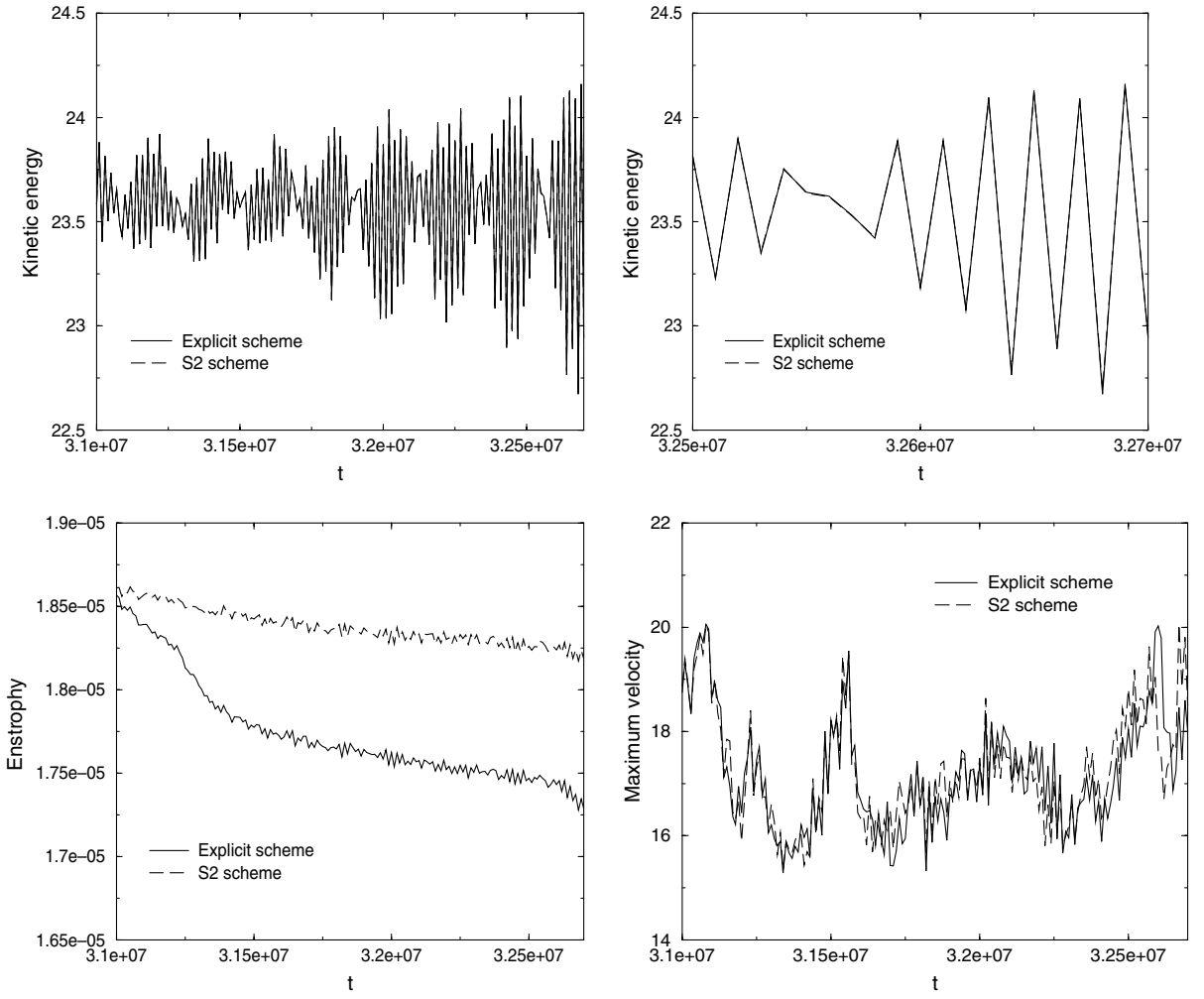

Fig. 11. Representation of the kinetic energy, the enstrophy, and the maximum velocity as functions of t.

with the S_2 and explicit reference schemes are quite similar, although the oscillations (high frequencies) around the profile are different.

In Fig. 12, we have represented the energy norm for the vorticity ω (see Fig. 12(a)), for the plane divergence δ (see Fig. 12(b)) and for the height h (see Figs. 12(c) and (d)). The behavior in time of the vorticity is similar with the enstrophy (see Fig. 11(c)). The other curves obtained with the S_2 scheme and with the explicit scheme are very similar in phase and in amplitude, over all the time integration (20 days), these results being better than with the semi-implicit and S_1 schemes (see Figs. 6 and 9). This is in agreement with the fact that the spectra of the height and plane divergence, corresponding to the explicit and S_2 schemes, are very similar for all the wavenumbers (see Fig. 10).

If we consider the time averages of the relative errors between the S_2 and explicit reference schemes, we see that the relative error on the kinetic energy $\|\mathbf{u}\|_{L^2(\Omega)}$ is around 8.7×10^{-5}, and the relative error on the energy norm of the height $\|h\|_{L^2(\Omega)}$ is approximately 1.0×10^{-3}, over the 20 days of the numerical comparison (see Table 1).

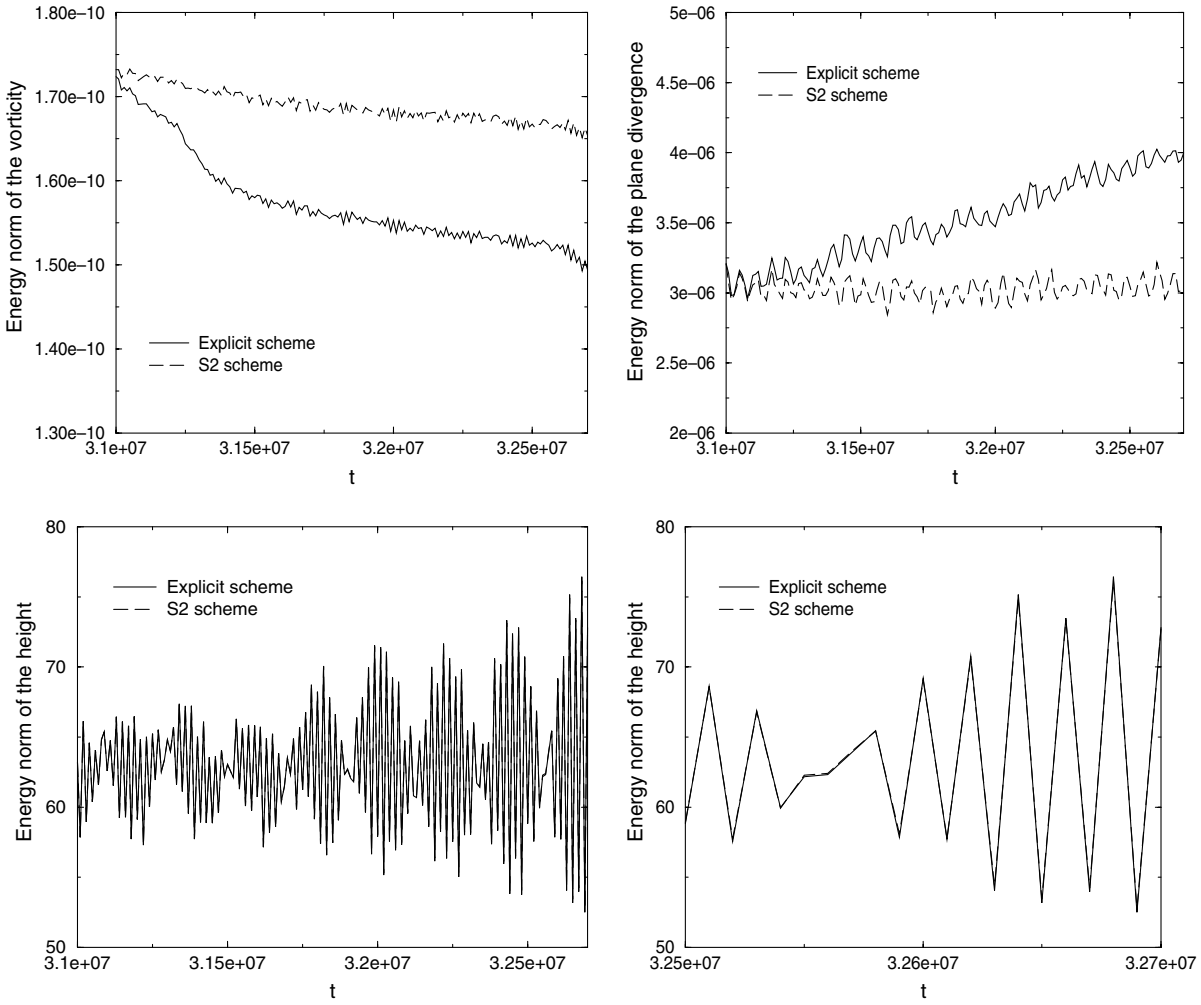

Fig. 12. Representation of the energy norm of the vorticity ω, of the plane divergence δ, and of the height h as functions of t.

Now, we shall compare the S_2 and the semi-implicit schemes, for a similar CPU time used. Let us consider the semi-implicit scheme (1.14) with a time step $\Delta t = 30$ s, instead of 50 s as previously. If we denote by $Nb_{\mathrm{i},30}$ the total number of operations used for the semi-implicit scheme ($\Delta t = 30$ s), over 20 days of simulation (namely 58,660 time steps), we have $Nb_{\mathrm{i},30} = \frac{5}{3}Nb_{\mathrm{i}} \simeq 33\%Nb_{\mathrm{Ref}} \simeq Nb_{S_2}$. In Figs. 13–15, we have compared the results obtained with the explicit reference scheme (1.9) for $\Delta t = \Delta t_{\mathrm{Ref}} = 10$ s as previously, and with the semi-implicit scheme (1.14) for $\Delta t = 30$ s.

Comparing Figs. 10 and 13, we see a better retranscription of the spectra with the S_2 scheme than with the semi-implicit scheme ($\Delta t = 30$ s), especially for the low and medium range of the spectra (large scales).

Similarly, comparing Figs. 11(a) and (b) and Figs. 14(a) and (b) (kinetic energy), we see that there is no decorrelation of the curves associated with the explicit and S_2 schemes, when the time increases, by opposition with the curves associated with the explicit and semi-implicit schemes ($\Delta t = 30$ s). The same

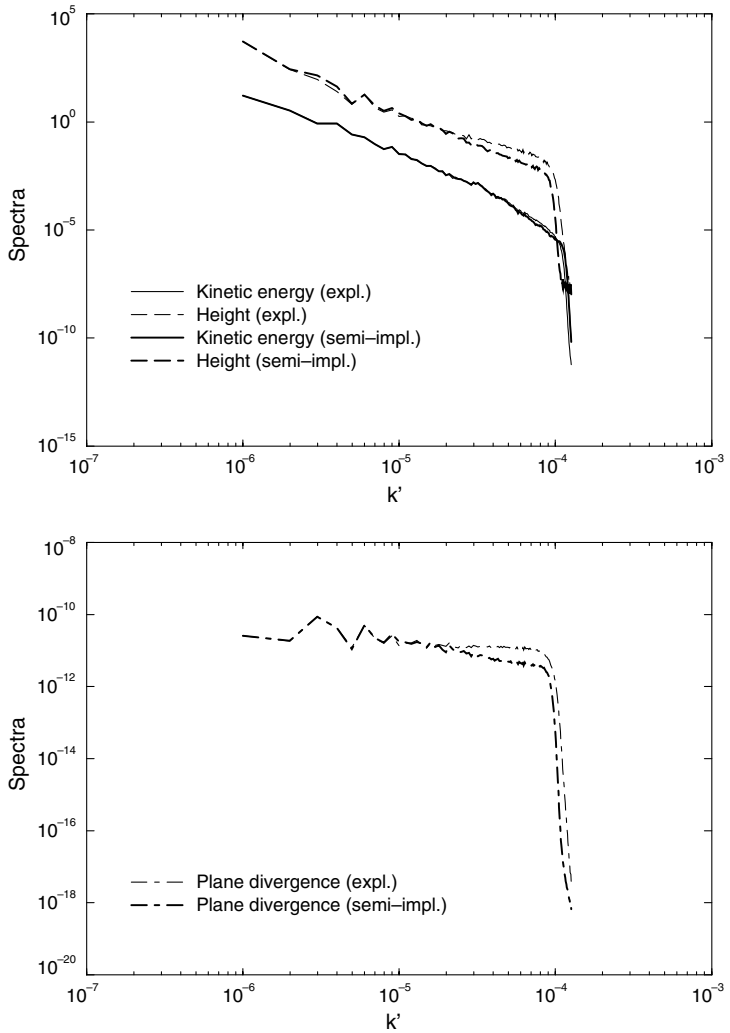

Fig. 13. Spectra of velocity (kinetic energy spectrum), height and plane divergence for the explicit reference scheme (thin lines) and for the semi-implicit scheme (thick lines). The semi-implicit scheme corresponds to the choice of $\Delta t = 30$ s.

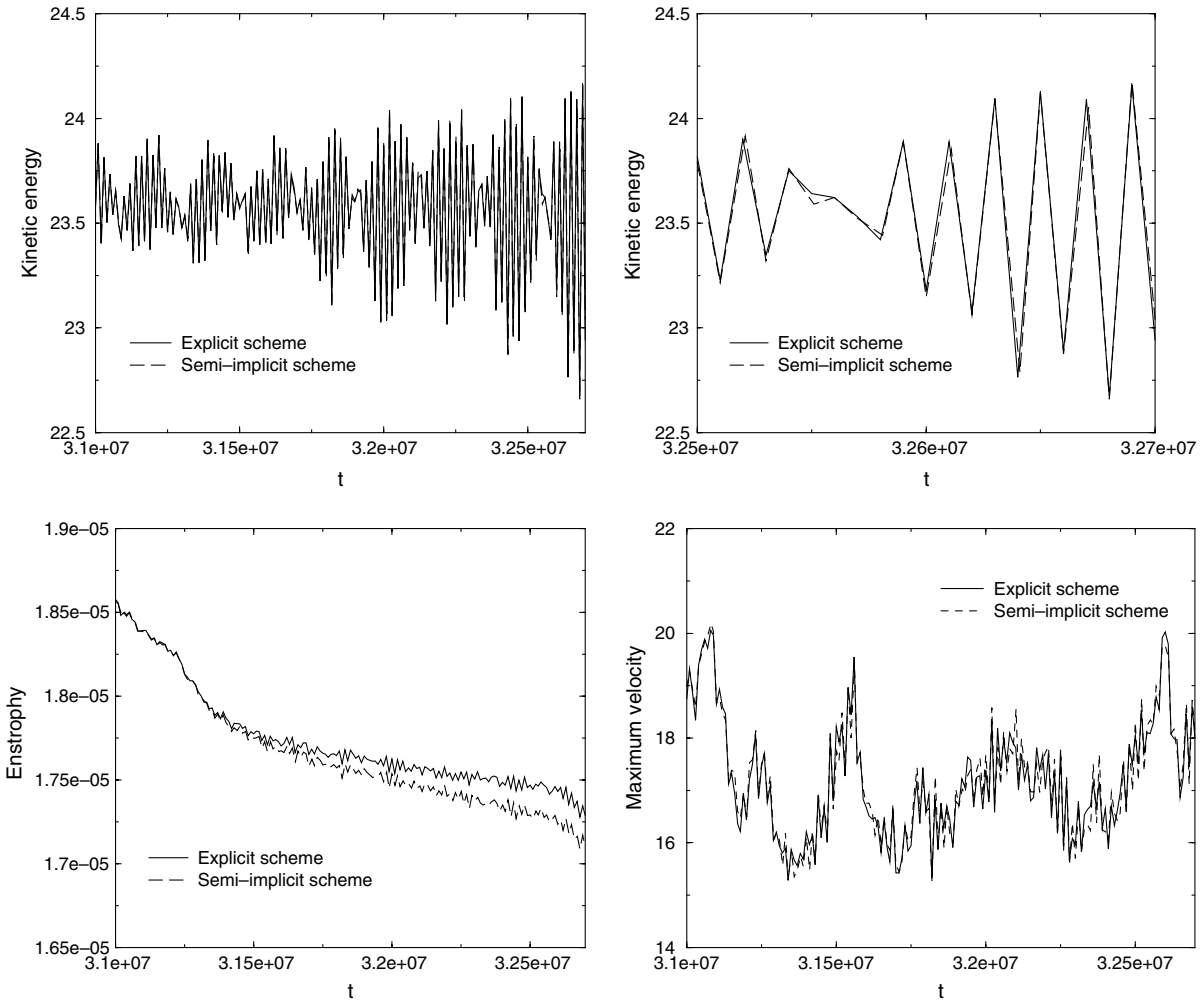

Fig. 14. Representation of the kinetic energy, the enstrophy, and the maximum velocity as functions of t. The semi-implicit scheme corresponds to the choice of $\Delta t = 30$ s.

comments are available, when we compare Figs. 12(c) and (d) and Figs. 15(c) and (d) (energy norm of the height): the height is well computed with the scheme S_2, when the time increases, with no decorrelation with the explicit reference scheme, by opposition with the semi-implicit scheme for $\Delta t = 30$ s.

If we consider the time averages of the relative errors between the semi-implicit scheme ($\Delta t = 30$ s) and explicit reference schemes, we see that the relative error on the kinetic energy $\|\mathbf{u}\|_{L^2(\Omega)}$ is around 2.2×10^{-4}, and the relative error on the energy norm of the height $\|h\|_{L^2(\Omega)}$ is approximately 2.7×10^{-3}, over the 20 days of the numerical comparison (see Table 1).

4. New schemes based on a splitting of the operators (multistep or fractional step methods)

Rather than new schemes based on a splitting of the scales, as previously considered in Sections 2 and 3 for the S_i schemes, $i = 1, 2$ (multilevel methods), we are now interested in developing new schemes based on

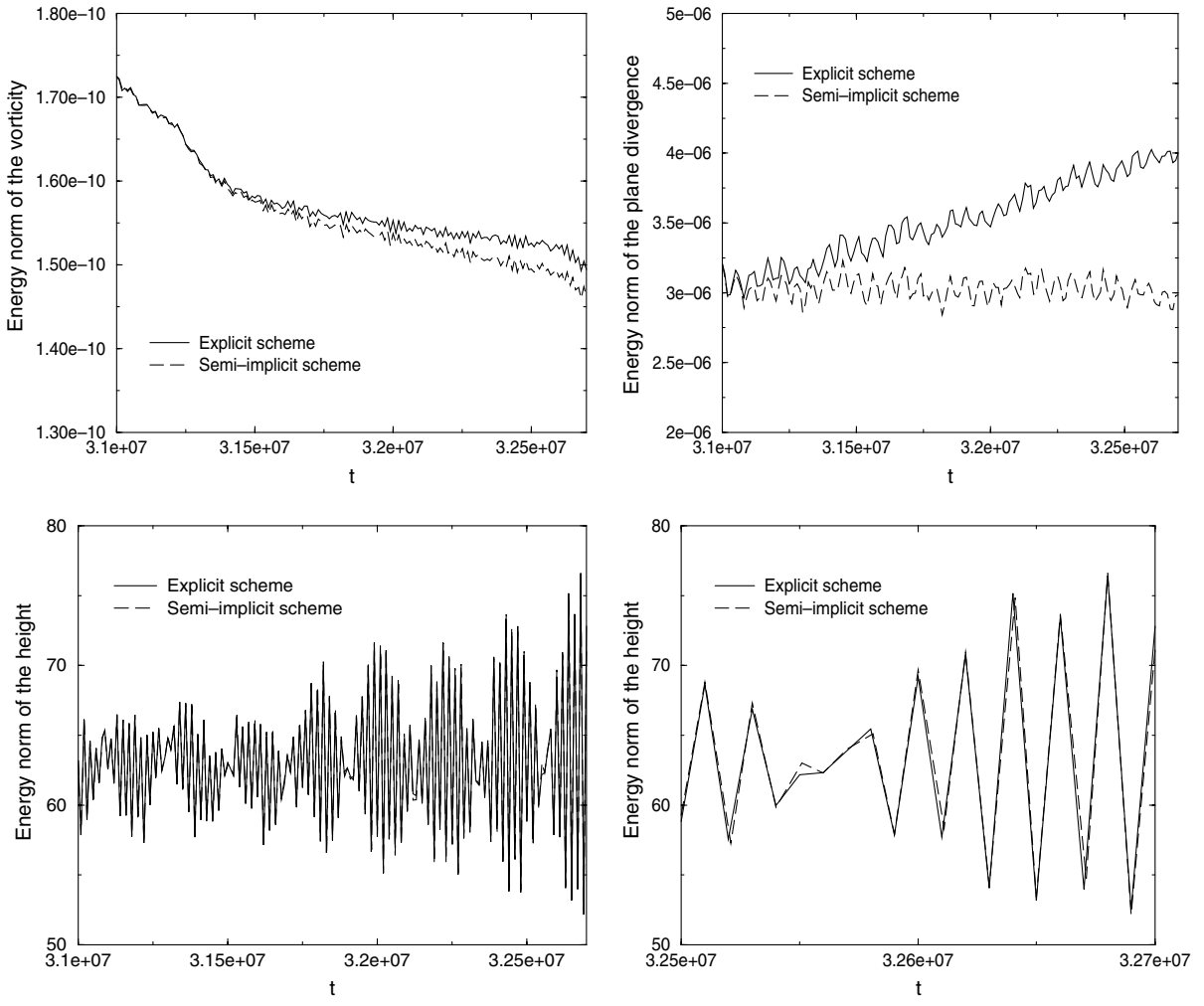

Fig. 15. Representation of the energy norm of the vorticity ω, of the plane divergence δ, and of the height h as functions of t. The semi-implicit scheme corresponds to the choice of $\Delta t = 30$ s.

a splitting of the operators (multistep schemes or fractional step schemes). Indeed, with the splitting of the operators, we can adapt the time integration to the terms considered in the equations. This is the object of this section.

4.1. A first fractional step scheme

The nonlinear terms are costly in CPU time, but the CFL stability constraint $Stab_1$ (see (1.11)), associated with the explicit time integration of the convective nonlinear terms, is not too restrictive. By opposition, the gravity terms are not costly in CPU time, but the stability constraint $Stab_3$ (see (1.13)), associated with the explicit time integration of these terms, is very restrictive (see Section 1). So, in order to take this into account, we propose to separate the time integration of the nonlinear terms and that of the gravity terms (separation of the operators), and to apply a specific time integration to the nonlinear terms and to the gravity terms. We call this a multistep or fractional step scheme.

To take into account separately the nonlinear terms and the gravity terms, one possibility is the following. To obtain $t_{n+1} = (n+1)\,\Delta t$ from $t_n = n\Delta t$, the time step Δt is decomposed as follows:

- first step: to take into account the nonlinear terms (and Coriolis terms) with the explicit Leap–Frog scheme (see (1.9)), over the time step Δt;
- n_b other steps, $n_b > 1$: to take into account the gravity terms with the explicit Leap–Frog scheme (see (1.9)), over the time step Δt.

So, we obtain the following scheme:

- Step one: $\forall \mathbf{k} \in \mathbb{I}_N$,

$$\begin{aligned}
\hat{\omega}_{\mathbf{k}}^{n+1} &= \exp(-2\nu_T \Delta t |\mathbf{k}'|^{4p})\hat{\omega}_{\mathbf{k}}^{n-1} - 2\Delta t \exp(-\nu_T \Delta t |\mathbf{k}'|^{4p})(\hat{T}_{\omega,N}^{n}(\mathbf{k}) + f\hat{\delta}_{\mathbf{k}}^{n}),\\
\hat{\tilde{\delta}}_{\mathbf{k}}^{1} &= \exp(-2\nu_T \Delta t |\mathbf{k}'|^{4p})\hat{\delta}_{\mathbf{k}}^{n-1} - 2\Delta t \exp(-\nu_T \Delta t |\mathbf{k}'|^{4p})(\hat{T}_{\delta,N}^{n}(\mathbf{k}) - f\hat{\omega}_{\mathbf{k}}^{n}),\\
\hat{\tilde{h}}_{\mathbf{k}}^{1} &= \exp(-2\nu_T \Delta t |\mathbf{k}'|^{4p})\hat{h}_{\mathbf{k}}^{n-1} - 2\Delta t \exp(-\nu_T \Delta t |\mathbf{k}'|^{4p})\hat{T}_{h,N}^{n}(\mathbf{k}).
\end{aligned} \tag{4.1}$$

- Step i, $i = 2,\ldots,n_b+1$: $\forall \mathbf{k} \in \mathbb{I}_N$,

$$\begin{aligned}
\hat{\tilde{\delta}}_{\mathbf{k}}^{i} &= \exp(-2\nu_T \Delta t |\mathbf{k}'|^{4p})\hat{\tilde{\delta}}_{\mathbf{k}}^{i-2} + 2\Delta t |\mathbf{k}'|^2 \frac{g}{n_b} \exp(-\nu_T \Delta t |\mathbf{k}'|^{4p})\hat{\tilde{h}}_{\mathbf{k}}^{i-1},\\
\hat{\tilde{h}}_{\mathbf{k}}^{i} &= \exp(-2\nu_T \Delta t |\mathbf{k}'|^{4p})\hat{\tilde{h}}_{\mathbf{k}}^{i-2} - 2\Delta t \frac{H}{n_b} \exp(-\nu_T \Delta t |\mathbf{k}'|^{4p})\hat{\tilde{\delta}}_{\mathbf{k}}^{i-1},
\end{aligned} \tag{4.2}$$

  with $\hat{\tilde{\delta}}_{\mathbf{k}}^{0} = \hat{\delta}_{\mathbf{k}}^{n-1}$ and $\hat{\tilde{h}}_{\mathbf{k}}^{0} = \hat{h}_{\mathbf{k}}^{n-1}$.
- Finally: $\forall \mathbf{k} \in \mathbb{I}_N$,

$$\begin{aligned}
\hat{\delta}_{\mathbf{k}}^{n+1} &= \hat{\tilde{\delta}}_{\mathbf{k}}^{n_b+1},\\
\hat{h}_{\mathbf{k}}^{n+1} &= \hat{\tilde{h}}_{\mathbf{k}}^{n_b+1}.
\end{aligned} \tag{4.3}$$

This scheme is a fractional time step, with $n_b + 1$ steps. As we can see on (4.2), taking into account the gravity terms over n_b sub-steps allows to reduce the influence of these terms at each step, since g and H are replaced by g/n_b and H/n_b, increasing the numerical stability. The time step is always the same Δt (see the hyperdissipative operator), and we use several steps, for one time step, to decrease the influence of the gravity terms at each step.

For the global consistency of the scheme on the δ and h equations, we have, summing (4.1) and (4.2), for $i = 3,\ldots,n_b+1$, i odd (we suppose that n_b is even): $\forall \mathbf{k} \in \mathbb{I}_N$,

$$\begin{aligned}
\exp(\nu_T \Delta t |\mathbf{k}'|^{4p})\hat{\delta}_{\mathbf{k}}^{n+1} + 2\mathrm{sh}(\nu_T \Delta t |\mathbf{k}'|^{4p}) \sum_{i=3}^{n_b-1} \hat{\tilde{\delta}}_{\mathbf{k}}^{i} &= \exp(-\nu_T \Delta t |\mathbf{k}'|^{4p})\hat{\delta}_{\mathbf{k}}^{n-1} - 2\Delta t(\hat{T}_{\delta,N}^{n}(\mathbf{k}) - f\hat{\omega}_{\mathbf{k}}^{n})\\
&\quad + 2\Delta t |\mathbf{k}'|^2 g \left\langle \hat{\tilde{h}}_{\mathbf{k}} \right\rangle_{n_b},\\
\exp(\nu_T \Delta t |\mathbf{k}'|^{4p})\hat{h}_{\mathbf{k}}^{n+1} + 2\mathrm{sh}(\nu_T \Delta t |\mathbf{k}'|^{4p}) \sum_{i=3}^{n_b-1} \hat{\tilde{h}}_{\mathbf{k}}^{i} &= \exp(-\nu_T \Delta t |\mathbf{k}'|^{4p})\hat{h}_{\mathbf{k}}^{n-1} - 2\Delta t \hat{T}_{h,N}^{n}(\mathbf{k}) - 2\Delta t H \left\langle \hat{\tilde{\delta}}_{\mathbf{k}} \right\rangle_{n_b},
\end{aligned} \tag{4.4}$$

where

$$\left\langle \hat{\tilde{\delta}}_{\mathbf{k}} \right\rangle_{n_b} = \frac{1}{n_b} \sum_{i=2}^{n_b} \hat{\tilde{\delta}}_{\mathbf{k}}^{\,i}, \quad i \text{ even},$$
$$\left\langle \hat{\tilde{h}}_{\mathbf{k}} \right\rangle_{n_b} = \frac{1}{n_b} \sum_{i=2}^{n_b} \hat{\tilde{h}}_{\mathbf{k}}^{\,i}, \quad i \text{ even}. \tag{4.5}$$

We have chosen $\zeta = 10^4$ and $p = 2$ (see Section 2). Moreover, we have $0 \leqslant v_T \Delta t |\mathbf{k}'|^{4p} \ll 1$, for essentially all the wavenumbers $\mathbf{k}'$. So, $\mathrm{sh}(v_T \Delta t |\mathbf{k}'|^{4p}) \simeq v_T\, \Delta t |\mathbf{k}'|^{4p} \ll 1$, for essentially all the wavenumbers $\mathbf{k}'$. Since the coefficients associated with $\hat{\delta}_{\mathbf{k}}^{n+1}$ (resp. $\hat{h}_{\mathbf{k}}^{n+1}$) and $\hat{\delta}_{\mathbf{k}}^{n-1}$ (resp. $\hat{h}_{\mathbf{k}}^{n-1}$) in (4.4) are, $\exp(\pm v_T \Delta t |\mathbf{k}'|^{4p}) \simeq 1 \pm v_T \Delta t |\mathbf{k}'|^{4p} \simeq 1$, we can neglect the action of the terms $2\mathrm{sh}(v_T \Delta t |\mathbf{k}'|^{4p}) \sum_{i=1}^{n_b} \hat{\tilde{\delta}}_{\mathbf{k}}^{\,i}$ and $2\mathrm{sh}(v_T \Delta t |\mathbf{k}'|^{4p}) \sum_{i=1}^{n_b} \hat{\tilde{h}}_{\mathbf{k}}^{\,i}$ in (4.4). Finally, for essentially all the wavenumbers $\mathbf{k}$, we obtain for the scheme (4.1)–(4.3):

$$\begin{aligned}
\hat{\omega}_{\mathbf{k}}^{n+1} &= \exp(-2 v_T \Delta t |\mathbf{k}'|^{4p}) \hat{\omega}_{\mathbf{k}}^{n-1} - 2\Delta t \exp(-v_T \Delta t |\mathbf{k}'|^{4p}) (\hat{T}_{\omega,N}^{n}(\mathbf{k}) + f \hat{\delta}_{\mathbf{k}}^{n}), \\
\hat{\delta}_{\mathbf{k}}^{n+1} &\simeq \exp(-2 v_T \Delta t |\mathbf{k}'|^{4p}) \hat{\delta}_{\mathbf{k}}^{n-1} - 2\Delta t \exp(-v_T \Delta t |\mathbf{k}'|^{4p}) \left(\hat{T}_{\delta,N}^{n}(\mathbf{k}) - f \hat{\omega}_{\mathbf{k}}^{n} - |\mathbf{k}'|^2 g \left\langle \hat{\tilde{h}}_{\mathbf{k}} \right\rangle_{n_b} \right), \\
\hat{h}_{\mathbf{k}}^{n+1} &\simeq \exp(-2 v_T \Delta t |\mathbf{k}'|^{4p}) \hat{h}_{\mathbf{k}}^{n-1} - 2\Delta t \exp(-v_T \Delta t |\mathbf{k}'|^{4p}) \left(\hat{T}_{h,N}^{n}(\mathbf{k}) + H \left\langle \hat{\tilde{\delta}}_{\mathbf{k}} \right\rangle_{n_b} \right).
\end{aligned} \tag{4.6}$$

Considering at $\hat{\tilde{\delta}}_{\mathbf{k}}^{\,i}$ and $\hat{\tilde{h}}_{\mathbf{k}}^{\,i}$, $i = 1, \ldots, n_b$, as estimates of $\hat{\delta}_{\mathbf{k}}(t)$ and $\hat{h}_{\mathbf{k}}(t)$, respectively, at intermediate times lying between t_n and t_{n+1}, we deduce from (4.5) that:

$$\left\langle \hat{\tilde{\delta}}_{\mathbf{k}} \right\rangle_{n_b} = \frac{1}{n_b} \sum_{i=2,\ i\text{even}}^{n_b} \hat{\tilde{\delta}}_{\mathbf{k}}^{\,i} \simeq \frac{1}{\Delta t} \int_{t_n}^{t_{n+1}} \hat{\delta}_{\mathbf{k}}(t)\, \mathrm{d}t,$$
$$\left\langle \hat{\tilde{h}}_{\mathbf{k}} \right\rangle_{n_b} = \frac{1}{n_b} \sum_{i=2,\ i\text{even}}^{n_b} \hat{\tilde{h}}_{\mathbf{k}}^{\,i} \simeq \frac{1}{\Delta t} \int_{t_n}^{t_{n+1}} \hat{\delta}_{\mathbf{k}}(t)\, \mathrm{d}t. \tag{4.7}$$

The temporal averages (4.7), over one time step Δt, for the gravity terms, induce a filtration of the high temporal frequencies, associated with the fast waves of the gravity terms, which are responsible for the numerical instability problems (see Section 1). So, we can hope to obtain a better numerical stability with such a scheme. Our fractional step schemes are different from the method of averages proposed in [42,31] and [23]. Indeed, in the fractional step schemes described here, we use a second order time scheme for all the scales and we update the size of the time step in function of the operator. In averaged methods, a second order time scheme with large time step is used for the slow variables, and a first order time scheme with small time step is used for the fast variables. The coupling between the slow and fast variables is obtained with time averaging.

4.2. Scheme S_3

Since the implicit Crank–Nicholson scheme is stable, but with a dispersive error (see Section 1), a variant of the previous fractional step scheme (4.1)–(4.3) is to use the Crank–Nicholson scheme, instead of the Leap–Frog scheme, over the n_b sub-steps for the gravity terms in (4.2). Like this, we can hope to benefit of the stability properties of the Crank–Nicholson scheme, and to reduce the dispersive error, by comparison with the semi-implicit scheme (1.14), since the influence of the gravity terms, on each sub-step, is reduced (the parameters g and H being divided by n_b). So, we obtain the following scheme, named S_3:

- Step one: $\forall \mathbf{k} \in \mathbb{I}_N$,

$$\begin{aligned}
\hat{\omega}_{\mathbf{k}}^{n+1} &= \exp(-2\nu_T \Delta t |\mathbf{k}'|^{4p}) \hat{\omega}_{\mathbf{k}}^{n-1} - 2\Delta t \exp(-\nu_T \Delta t |\mathbf{k}'|^{4p})(\hat{T}_{\omega,N}^{n}(\mathbf{k}) + f\hat{\delta}_{\mathbf{k}}^{n}), \\
\hat{\tilde{\delta}}_{\mathbf{k}}^{1} &= \exp(-2\nu_T \Delta t |\mathbf{k}'|^{4p}) \hat{\delta}_{\mathbf{k}}^{n-1} - 2\Delta t \exp(-\nu_T \Delta t |\mathbf{k}'|^{4p})(\hat{T}_{\delta,N}^{n}(\mathbf{k}) - f\hat{\omega}_{\mathbf{k}}^{n}), \\
\hat{\tilde{h}}_{\mathbf{k}}^{1} &= \exp(-2\nu_T \Delta t |\mathbf{k}'|^{4p}) \hat{\delta}_{\mathbf{k}}^{n-1} - 2\Delta t \exp(-\nu_T \Delta t |\mathbf{k}'|^{4p}) \hat{T}_{h,N}^{n}(\mathbf{k}).
\end{aligned} \tag{4.8}$$

- Step i, $i = 2, \ldots, n_b + 1$: $\forall \mathbf{k} \in \mathbb{I}_N$,

$$\begin{aligned}
\hat{\tilde{\delta}}_{\mathbf{k}}^{i} - \frac{g}{n_b}\Delta t |\mathbf{k}'|^2 \hat{\tilde{h}}_{\mathbf{k}}^{i} &= \exp(-2\nu_T \Delta t |\mathbf{k}'|^{4p}) \hat{\tilde{\delta}}_{\mathbf{k}}^{i-2} + \Delta t |\mathbf{k}'|^2 \frac{g}{n_b} \exp(-2\nu_T \Delta t |\mathbf{k}'|^{4p}) \hat{\tilde{h}}_{\mathbf{k}}^{i-2}, \\
\hat{\tilde{h}}_{\mathbf{k}}^{i} + \frac{H}{n_b}\Delta t \hat{\tilde{\delta}}_{\mathbf{k}}^{i} &= \exp(-2\nu_T \Delta t |\mathbf{k}'|^{4p}) \hat{\tilde{h}}_{\mathbf{k}}^{i-2} - \Delta t \frac{H}{n_b} \exp(-2\nu_T \Delta t |\mathbf{k}'|^{4p}) \hat{\tilde{\delta}}_{\mathbf{k}}^{i-2},
\end{aligned} \tag{4.9}$$

  with $\hat{\tilde{\delta}}_{\mathbf{k}}^{0} = \hat{\delta}_{\mathbf{k}}^{n}$ and $\hat{\tilde{h}}_{\mathbf{k}}^{0} = \hat{h}_{\mathbf{k}}^{n}$.

- Finally: $\forall \mathbf{k} \in \mathbb{I}_N$,

$$\begin{aligned}
\hat{\delta}_{\mathbf{k}}^{n+1} &= \hat{\tilde{\delta}}_{\mathbf{k}}^{n_b+1}, \\
\hat{h}_{\mathbf{k}}^{n+1} &= \hat{\tilde{h}}_{\mathbf{k}}^{n_b+1}.
\end{aligned} \tag{4.10}$$

5. Numerical results (multistep or fractional step method)

In this section we shall present the numerical results obtained with the new multistep scheme S_3 described in Section 4.

As with the multilevel schemes (see Section 3), our aim is to obtain new schemes to resolve the shallow water problem (1.5), with less CPU time used than for the explicit scheme (1.9), and with an acceptable dispersive error. Ideally, as in Section 3, we want through the new proposed schemes, to be able to compute the numerical solution of (1.5), with approximately the accuracy of the explicit scheme (1.9), and with nearly the CPU time of the semi-implicit scheme (1.14).

We compare the S_3 scheme (see Section 4.2) with the explicit reference scheme (1.9). We have chosen a time step $\Delta t = 3\,\Delta t_{\mathrm{Ref}} = 30$ s. As for the parameter n_b, we have chosen $n_b = 10$. Let us consider the total number of operations Nb_{S_3} required for the S_3 scheme, over 20 days of simulation (i.e., 58,660 time steps). Since the CPU time used is essentially due to nonlinear terms computation, and since the nonlinear terms are computed only at the first substep (Step one, see (4.8)), we have $Nb_{S_3} \simeq Nb_{\mathrm{i},30} = \frac{5}{3} Nb_{\mathrm{i}} \simeq 33\% Nb_{\mathrm{Ref}} \simeq Nb_{S_2}$.

In Fig. 16, we have represented the spectra of the velocity field, of the height and of the plane divergence. Except for the highest wavenumbers, the spectra obtained with the S_3 scheme are very similar with those corresponding to the explicit scheme.

Then, we consider, in Fig. 17, the kinetic energy (see Figs. 17(a) and (b)), the enstrophy (see Fig. 17(c)) and the maximum velocity (see Fig. 17(d)), computed with the explicit reference scheme and with the S_3 scheme. As we can see, the results obtained with the S_3 scheme are very similar with those obtained with the explicit reference scheme, and so better than with the semi-implicit scheme with a time step of 50 s (see Figs. 5(a) and (b)). In particular, for the maximum velocity in Fig. 17(d), the correlation between the explicit and S_3 curves is good, over all the time interval.

In Fig. 18, we have represented the energy norm for the vorticity ω (see Fig. 18(a)), for the plane divergence δ (see Fig. 18(b)) and for the height h (see Figs. 18(c) and (d)). The behavior of the vorticity, in time, is

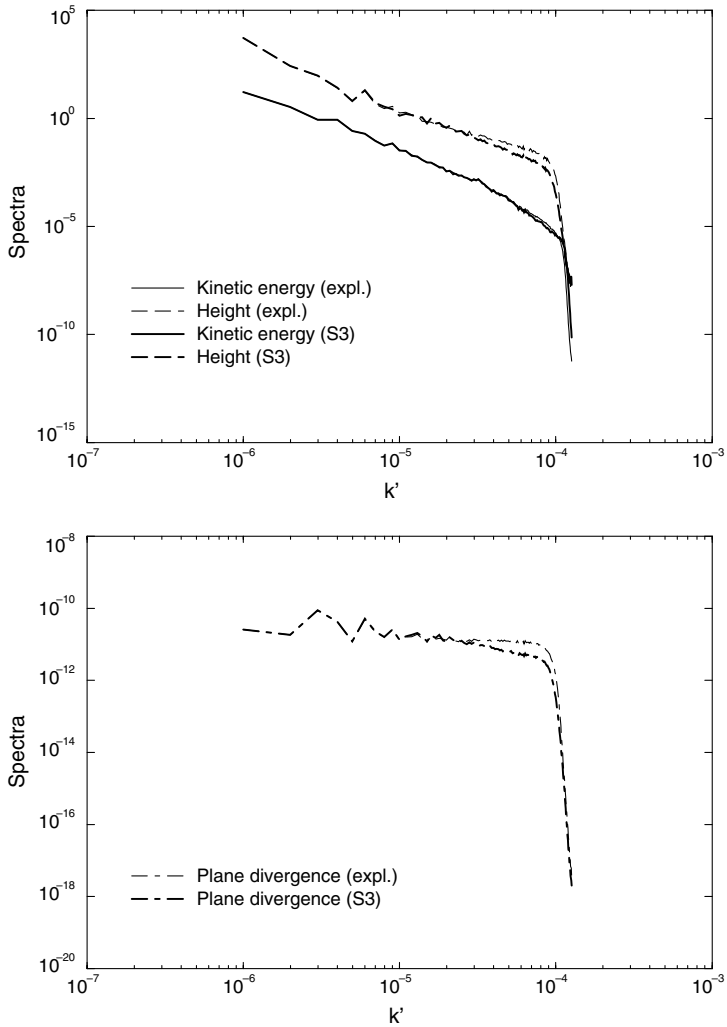

Fig. 16. Spectra of velocity (kinetic energy spectrum), height and plane divergence for the explicit reference scheme (thin lines) and for the scheme S_3 (thick lines).

similar with the enstrophy (see Fig. 17(c)). In Fig. 17(b), we can see the good agreement of the results obtained with the explicit scheme and with the S_3 scheme, for the plane divergence. As for the height, we see in Figs. 17(c) and (d) that the explicit and S_3 curves are very similar, over all the time, as it was the case for the S_2 scheme (see Figs. 12(c) and (d)).

If we consider the time averages of the relative errors between the S_3 and explicit reference schemes, we see that the relative error on the kinetic energy $\|\mathbf{u}\|_{L^2(\Omega)}$ is around 3.3×10^{-4}, and the relative error on the energy norm of the height $\|h\|_{L^2(\Omega)}$ is approximately 2.6×10^{-3}, over the 20 days of the numerical comparison (see Table 1).

We have previously seen that the S_3 scheme required a CPU time of the same order as for the S_2 scheme (see Section 3.4) and for the semi-implicit scheme with a time step $\Delta t = 30$ s (see Section 3.4). We can compare the S_3 and S_2 schemes through Figs. 10–12 and Figs. 16–18. Similarly, we can compare the S_3 scheme with the semi-implicit scheme with a time step $\Delta t = 30$ s through Figs. 13–15 and Figs. 16–18. Finally, as it

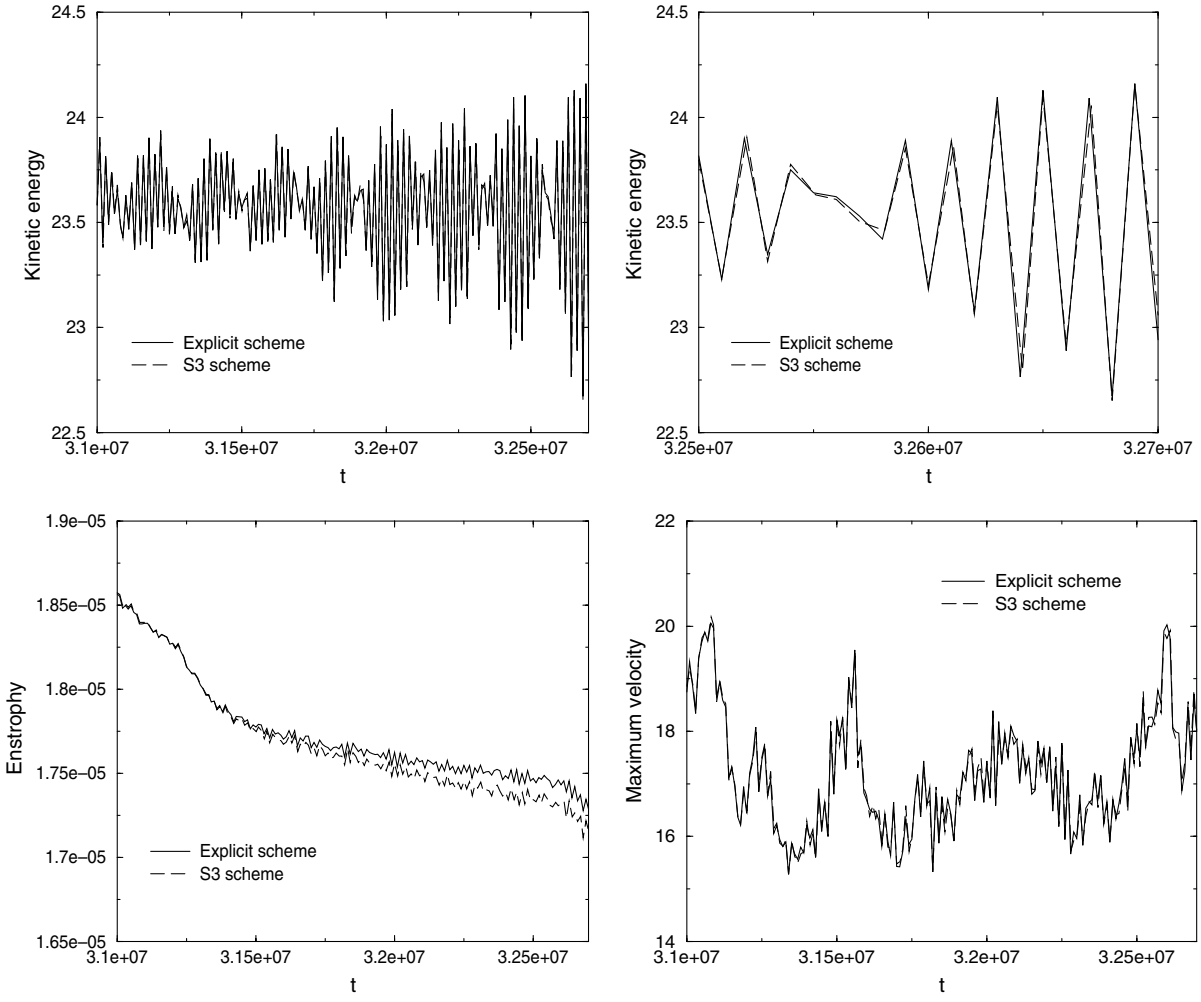

Fig. 17. Representation of the kinetic energy, the enstrophy, and the maximum velocity as functions of t.

has been said before, we recall that the time averages of the relative errors, over the 20 days of the numerical comparison, between the S_2 scheme (resp. the semi-implicit scheme with a time step $\Delta t = 30s$) and the explicit reference scheme is 8.7×10^{-5} (resp. 2.2×10^{-4}) for the kinetic energy, and 1.0×10^{-3} (resp. 2.7×10^{-3}) for the energy norm of the height (see Section 3.4). For more complete comparisons, see Table 1.

6. Conclusion and future work

We have presented in this work several new multilevel/multistep schemes to compute the numerical solution of the shallow water problem (1.5). These schemes are based on a scale separation (multilevel methods), or an operator separation (multistep or fractional step methods). The numerical results obtained show that the schemes proposed allow to reduce the dispersive error and to increase the numerical stability.

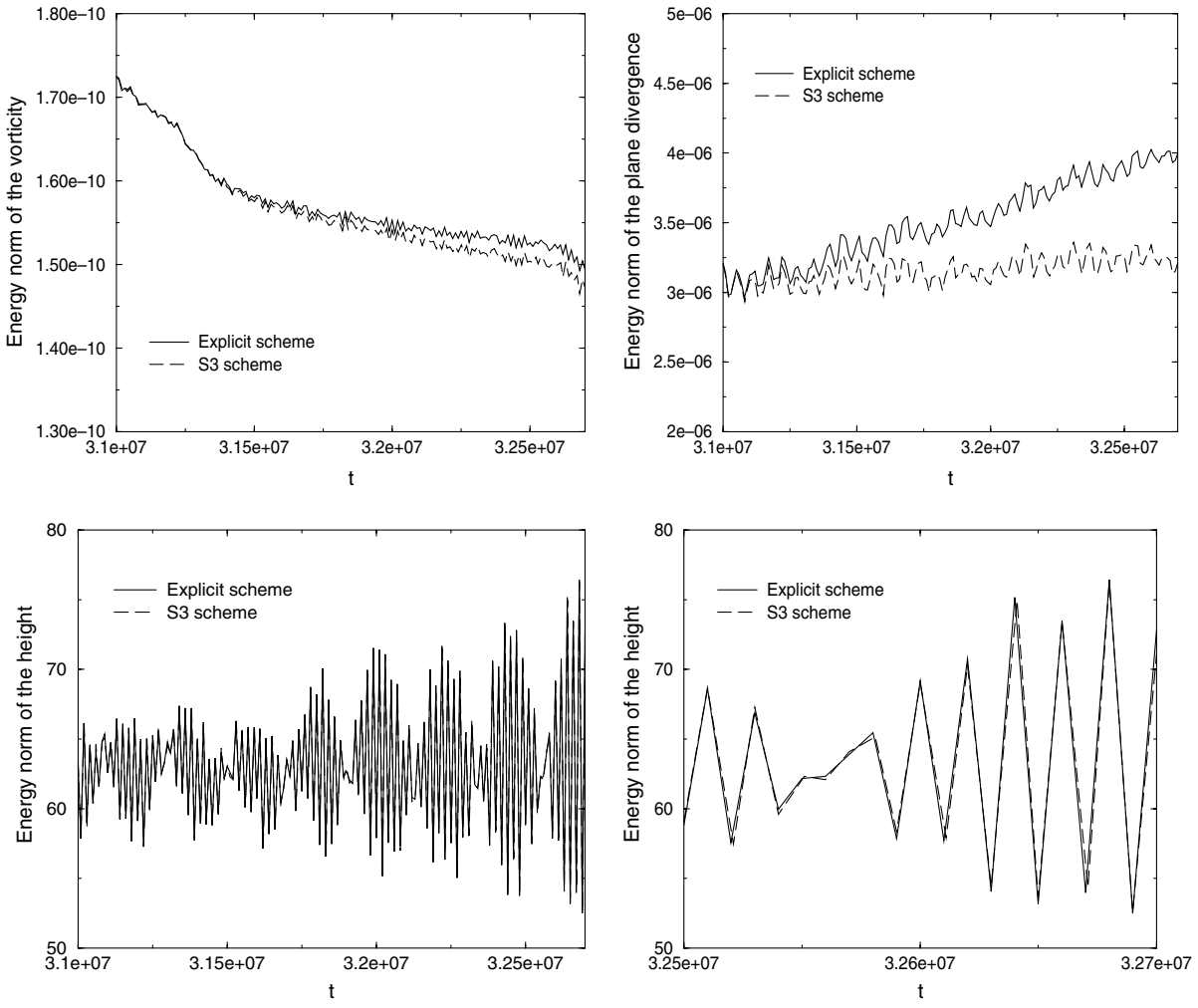

Fig. 18. Representation of the energy norm of the vorticity ω, of the plane divergence δ, and of the height h as functions of t.

It is possible to consider the splitting of the scales, used in Section 2, with the splitting of the operators, used in Section 4. Since the stability constraint of the time integration of the gravity terms is stronger for the high wavenumbers (small scales) than for the low wavenumbers (large scales), see Section 1, we can think at separating the scales (splitting of the scales), and adapting the parameter n_b, used in the previous multistep schemes (4.1)–(4.3) and S_3 (splitting of the operators), as function of the size of the scales computed. The parameter n_b will be chosen larger for the small wavenumbers than for the large wavenumbers. Moreover, we use the explicit Leap–Frog scheme (resp. the implicit Crank–Nicholson scheme) for the small wavenumbers (resp. large wavenumbers). We shall denote by $n_{b,\mathrm{expl}}$ (resp. $n_{b,\mathrm{impl}}$) the value of the parameter n_b chosen to compute the large (resp. small) scales, with the explicit (1.9) (resp. semi-implicit (1.14)) scheme. So, to compute the large scales, we obtain an explicit multistep scheme with $n_{b,\mathrm{expl}} + 1$ steps. As for the small scales, we obtain a semi-implicit multistep scheme with $n_{b,\mathrm{impl}} + 1$ steps.

Another planetary model is the two-dimensional shallow water problem on the sphere (spherical coordinates). In this case, an additional problem is the use of nonuniform meshes (finer near the poles, see [49],

for example). So, the presence of the poles implies a more restrictive stability constraint over all the sphere. To overcome this, we can use spectral methods with spherical harmonic basis. For more details, see [18,33,34,48,49]. We intend to adapt the new multilevel and multistep schemes previously described to this case of a spherical geometry.

We shall also consider the case of the system of equations (1.2) on a rectangular domain Ω, with Dirichlet boundary conditions. This problem is considered as a limited area model (LAM) in meteorology, also called regional problem (see [43,13]). The numerical approximation is often obtained using a finite difference method. Such a model allows, in meteorology, a prediction for the small scales on a short period, by opposition with a planetary model, which is used for the prediction of the large scales on a long period. Indeed, in the case of a limited area model, the mesh is finer than for a planetary model. For a LAM, it is necessary to specify the values of the velocity field on the boundary of the limited area domain (Dirichlet boundary conditions), at each time step. These values, on the boundary, can be obtained using a model for the large scales (for example a planetary model). For more details, see, for example [13,43]. However, due to the hyperbolic character of the shallow water equations (1.2), the boundary conditions cannot be applied everywhere on the boundary $\partial\Omega$ of the rectangular domain Ω. The localization of the boundary conditions is function of the characteristic values: $|\mathbf{U}|$ and $|\mathbf{U}| \pm \sqrt{gH + \frac{f^2}{k^2}}$ in the linearized case (characteristic method), i.e., of the wave propagation. According the value of the height parameter H, the characteristic values have different signs. So, the number of characteristics which enter in the domain is different. For more details on this problem of boundary conditions, see [32,45,47]. We also intend to adapt the previous multilevel and multistep schemes, to the case of a limited area model. To obtain large and small scales decomposition in the finite difference case or in the finite volume case, we will use the incremental unknowns (IU). For more details on the incremental unknowns see, for example [9–12,20] and the references therein. This work is in progress (see [17]) and will be presented elsewhere.

Acknowledgments

This work was supported in part by NSF-DMS grants 00-74334 and 03-05110 and by the Research Fund of Indiana University. It was initiated during the visit of Joe Tribbia, at the Applied Mathematics Laboratory of Clermont-Ferrand 2 University (France), and at the Mathematics Laboratory of Paris Sud University (Orsay, France). The computations were performed on the Alpha Station XP1000 of the Mathematics Laboratory of Nantes University (France), and on the IBM SP of the Supercomputing Center IDRIS of CNRS (France). The authors thank the Reviewers for their very useful comments.

References

[2] P. Bartello, A comparison of time discretization schemes for two-timescale problems in geophysical fluid dynamics, J. Comput. Phys. 179 (2002) 268–285.
[3] C. Basdevant, B. Legras, R. Sadourny, M. Béland, A study of barotropic model flows: intermittency, waves and predictability, J. Atmos. Sci. 38 (11) (1981) 2305–2326.
[4] G.K. Batchelor, The Theory of Homogeneous Turbulence, Cambridge University Press, Cambridge, 1971.
[5] G.L. Browning, J.J. Hack, P.N. Swarztrauber, A comparison of three numerical methods for solving differential equations on the sphere, Mon. Weather Rev. 117 (1989) 1058–1075.
[6] G.L. Browning, H.O. Kreiss, Comparison of numerical methods for the calculation of two-dimensional turbulence, Math. Comput. 52 (186) (1989) 369–388.
[7] G.L. Browning, H.O. Kreiss, Splitting methods for problems with different time scales, Mon. Weather Rev. 122 (1994) 2614–2622.
[8] C. Canuto, Y. Hussaini, A. Quarteroni, T.A. Zang, Spectral Methods in Fluid Dynamics, Springer, New York, 1988.
[9] J.P. Chehab, B. Costa, Time explicit schemes and spatial finite differences splittings, J. Sci. Comput. 20 (2) (2004) 159–189.

[10] J.P. Chehab, A. Miranville, Incremental unknowns method on nonuniform meshes, Math. Model. Numer. Anal. (M2AN) 32 (5) (1998) 539–577.
[11] M. Chen, A. Miranville, R.M. Temam, Incremental unknowns in finite differences in three space dimension, Comput. Appl. Math. 14 (3) (1995) 1–15.
[12] M. Chen, R.M. Temam, Incremental unknowns for solving partial differential equations, Numer. Math. 59 (1991) 255–271.
[13] J. Coiffier, Un demi-siècle de prévision numérique du temps, La Météorologie 8 (30) (2000) 11–31.
[14] B. Cushman-Roisin, Introduction to Geophysical Fluid Dynamics, Prentice-Hall, Englewood Cliffs, NJ, 1994.
[15] T. Dubois, F. Jauberteau, A dynamical multilevel model for the simulation of the small structures in three-dimensional homogeneous isotropic turbulence, J. Sci. Comput. 13 (3) (1998) 323–367.
[16] T. Dubois, F. Jauberteau, R.M. Temam, Dynamic Multilevel Methods and the Numerical Simulation of Turbulence, Cambridge University Press, Cambridge, 1999.
[17] T. Dubois, F. Jauberteau, R.M. Temam, in: E. Stein, R. de Borst, T. Hughes (Eds.), Multilevel Methods in Turbulence, Encyclopedia of Computational Mechanics, Wiley, New York, 2004.
[18] D.R. Durran, Numerical Methods for Wave Equations in Geophysical Fluid DynamicsTexts in Applied Mathematics, vol. 32, Springer, New York, 1999.
[19] A.J. Gadd, A split explicit integration scheme for numerical weather prediction, Quart. J. R. Met. Soc. 104 (1978) 569–582.
[20] S. Faure, Méthodes de volumes finis et multiniveaux pour les équations de Navier–Stokes, de Burgers et de la chaleur, Ph.D. Thesis, Université d'Orsay, 2003.
[21] A. Gelb, J.P. Gleeson, Spectral viscosity for shallow water equations in spherical geometry, Mon. Weather Rev. 129 (2001) 2346–2360.
[22] D. Gottlieb, S.A. Orszag, Numerical Analysis of Spectral Methods: Theory and ApplicationsCBMS-NSF regional conference series in applied mathematics, SIAM, Philadelphia, 1977.
[23] W.W. Grabowski, P.K. Smolarkiewicz, A multiscale anelastic model for meteorological research, Mon. Weather Rev. 130 (2002) 939–956.
[24] F. Jauberteau, R.M. Temam, Estimates based on scale separation for geophysical flows, Rev. R. Acad. Cien. Serie A. Mat. (RACSAM) 96 (3) (2002) 1–35.
[25] J.B. Klemp, R. Wilhelmson, The simulation of three-dimensional convective storm dynamics. Estimates based on scale separation for geophysical flows, J. Atmos. Sci. 35 (1978) 1070.
[26] D.A. Knoll, L. Chacon, L.G. Margolin, V.A. Mousseau, On balanced approximations for time integration of multiple time scale systems, J. Comput. Phys. 185 (2003) 583–611.
[27] R.H. Kraichnan, Inertial ranges in two-dimensional turbulence, Phys. Fluids 10 (1967) 1417–1423.
[28] J.L. Lions, R.M. Temam, S. Wang, Splitting up methods and numerical analysis of some multiscale problem, Int. J. Comput. Fluid Dyn. 5 (2) (1996) 157–202.
[29] R.J. LeVeque, J. Oliger, Numerical methods based on additive splittings for hyperbolic partial differential equations, Math. Comput. 40 (162) (1983) 469–497.
[30] G.I. Marchuk, Numerical Methods in Weather Prediction, Academic Press, New York, 1974.
[31] B.T. Nadiga, M.W. Hecht, L.G. Margolin, P.K. Smolarkiewicz, On simulating flows with multiple time scales using a method of averages, Theoret. Comput. Fluid Dyn. 9 (1997) 281–292.
[32] J. Oliger, A. Sundström, Theoretical and practical aspects of some initial boundary value problems in fluid mechanics, SIAM J. Appl. Math. 35 (3) (1978) 419–446.
[33] S.A. Orszag, Transform method for the calculation of vector-coupled sums: application to the spectral form of the vorticity equation, J. Atmos. Sci. 27 (1970) 890–895.
[34] S.A. Orszag, Fourier series on spheres, Mon. Weather Rev. 102 (1974) 56–75.
[35] F. Pascal, C. Basdevant, Nonlinear Galerkin method and subgrid model for two-dimensional turbulent flows, Theoret. Comput. Fluid Dyn. 3 (5) (1992) 267–284.
[36] U. Piomelli, Large-eddy simulation: present state and future directions, AIAA Paper 98-0534, 1998.
[37] P.J. Roache, Fundamentals of Computational Fluid Dynamic, Hermosa publishers, Albuquerque, NM, 1998.
[38] A.J. Robert, A stable numerical integration scheme for the primitive meteorological equations, Atmosphere-Ocean 19 (1) (1981) 35–46.
[39] P. Sagaut, Large Eddy Simulation for Incompressible Flows: an Introduction, Springer, Berlin, 2001.
[40] W.C. Skamarock, J.B. Klemp, The stability of time-split numerical methods for the hydrostatic and the nonhydrostatic elastic equations, Mon. Weather Rev. 120 (1992) 2109–2127.
[41] W.C. Skamarock, J.B. Klemp, Efficiency and accuracy of the Klemp–Wilhelmson time-splitting technique, Mon. Weather Rev. 122 (1994) 2623–2630.
[42] P.K. Smolarkiewicz, L.G. Margolin, On forward-in-time differencing for fluids: extension to a curvilinear framework, J. Mon. Weather Rev. 121 (1993) 1847–1859.

[43] A. Sundström, T. Elvius, Computational problems related to limited area modeling, GARP Publications Series, WMO and ICSU, Geneva 1979; 17(2) 379–416.
[44] E. Tadmor, Approximate solutions of nonlinear conservation laws, CIME course on "Advanced Numerical Approximation of Nonlinear Hyperbolic Equations", Cetraro, Italy, 1997.
[45] R.M. Temam, J. Tribbia, Open boundary conditions for the primitive and Boussinesq equations, J. Atmos. Sci. 60 (21) (2003) 2647–2660.
[46] C.B. Vreugdenhil, Numerical Methods for Shallow-water Flow, Kluwer Academic Publishers, Dordrecht, 1994.
[47] T.T. Warner, R.A. Peterson, R.E. Treadon, A tutorial on lateral boundary conditions as a basic and potentially serious limitation to regional numerical weather prediction, Bull. Am. Meteorol. Soc. 78 (11) (1997) 2599–2617.
[48] D.L. Williamson, J.T. Kiehl, V. Ramanathan, R.E. Dickinson, J.J. Hack, Description of NCAR community climate model (CCM1), NCAR Technical Note, NCAR/TN 285, 1987.
[49] D.L. Williamson, R. Laprise, in: K. Browning, R.J. Gurney (Eds.), Numerical Approximation for Global Atmospheric General Circulation Models, Cambridge University Press, Cambridge, 1999.